JOURNAL OF GEOPHYSICAL RESEARCH, VOL. 98, NO. B11, PAGES 19,533–19,563, NOVEMBER 10, 1993

Petrology and Geochemistry of the Galápagos Islands: Portrait of a Pathological Mantle Plume

WILLIAM M. WHITE

Department of Geological Sciences, Cornell University, Ithaca, New York

ALEXANDER R. MCBIRNEY

Center for Volcanology, University of Oregon, Eugene

ROBERT A. DUNCAN

College of Oceanography, Oregon State University, Corvallis

We report new major element, trace element, isotope ratio, and geochronological data on the Galápagos Archipelago. Magmas erupted from the large western volcanos are generally moderately fractionated tholeiites of uniform composition; those erupted on other islands are compositionally diverse, ranging from tholeiites to picritic basanitoids. While these volcanos do not form a strictly linear age progressive chain, the ages of the oldest dated flows on any given volcano do form a reasonable progression from youngest in the west to oldest in the east, consistent with motion of the Nazca plate with respect to the fixed hotspot reference frame. Isotope ratios in the Galápagos display a considerable range, from values typical of mid-ocean ridge basalt on Genovesa ($^{87}Sr/^{86}Sr$: 0.70259, ε_{Nd}: +9.4, $^{206}Pb/^{204}Pb$: 18.44), to typical oceanic island values on Floreana ($^{87}Sr/^{86}Sr$: 0.70366, ε_{Nd}: +5.2, $^{206}Pb/^{204}Pb$: 20.0). La/Sm_N ranges from 0.45 to 6.7; other incompatible element abundances and ratios show comparable ranges. Isotope and incompatible element ratios define a horseshoe pattern with the most depleted signatures in the center of the Galápagos Archipelago and the more enriched signatures on the eastern, northern, and southern periphery. These isotope and incompatible element patterns appear to reflect thermal entrainment of asthenosphere by the Galápagos plume as it experiences velocity shear in the uppermost asthenosphere. Both north-south heterogeneity within the plume itself and regional variations in degree and depth of melting also affect magma compositions. Rare earth systematics indicate that melting beneath the Galápagos begins in the garnet peridotite stability field, except beneath the southern islands, where melting may occur entirely in the spinel peridotite stability field. The greatest degree of melting occurs beneath the central western volcanos and decreases both to the east and to the north and south. $Si_{8.0}$, $Fe_{8.0}$, and $Na_{8.0}$ values are generally consistent with these inferences. This suggests that interaction between the plume and surrounding asthenosphere results in significant cooling of the plume. Superimposed on this thermal pattern produced by plume-asthenosphere interaction is a tendency for melting to be less extensive and to occur at shallower depths to the south, presumably reflecting a decrease in ambient asthenospheric temperatures away from the Galápagos Spreading Center.

INTRODUCTION

Production of basaltic magmas over stationary, long-lived hotspots in ocean basins is now generally thought to be a manifestation of rising convective plumes in the mantle [*Morgan*, 1971]. The longevity of such hotspots, their stationary nature, the simple age progression of volcanism in the island chains, and the geochemical distinctions between oceanic island basalts (OIB) and mid-ocean ridge basalts (MORB) are among the most convincing evidence in support of the convective plume theory.

Not all oceanic islands conform to this simple pattern. Among the most exceptional island groups is the Galápagos, which consists of 10 major volcanic islands and a number of lesser remnant volcanos that emerge from a broad, shallow submarine platform (Figure 1). While two aseismic ridges, the Cocos and Carnegie ridges, extend from the Galápagos Archipelago in the direction of Cocos and Nazca plate motions, the emergent volcanos do not form a linear chain. Nor is there any simple geographic pattern to the ages of the volcanos, although the oldest volcanos tend to occur in the southeast area of the archipelago. Of the 21 emergent volcanos in the Galápagos, nine have been active historically and four others have erupted in the Holocene and should be considered still active. By comparison, only six Hawaiian volcanos are active, and these are aligned in two chains with a clear age progression. The Galápagos Islands are also exceptional geochemically: while most basalts have typical OIB incompatible element concentrations and isotope ratios, basalts that are essentially indistinguishable from MORB in their geochemistry are also common products of Galápagos volcanos [*Baitis and Swanson*, 1976; *White and Hofmann*, 1978].

We report the results of a petrological and geochemical reconnaissance of the Galápagos Islands, including Sr, Nd, and Pb isotopic analyses of 124 samples, as well as trace and major element analyses, and 38 K-Ar age determinations. Our results suggest that the unique features of Galápagos volcanism reflect the local plate tectonic environment, and thermal and dynamic interaction between the asthenosphere and a mantle plume undergoing velocity shear. Tectonic factors control the location, size, and style of volcanism. Thermal interaction between plume and asthenosphere results in asthenosphere being entrained into the center of the plume. This, and the consequent plume-asthenosphere mixing, produces much of the observed geochemical variation. Superimposed on this mixing are variations in depth and degree of melting which also result from thermal interaction between plume and asthenosphere.

Paper number 93JB02018.
0148-227/93/93JB-02018$05.00

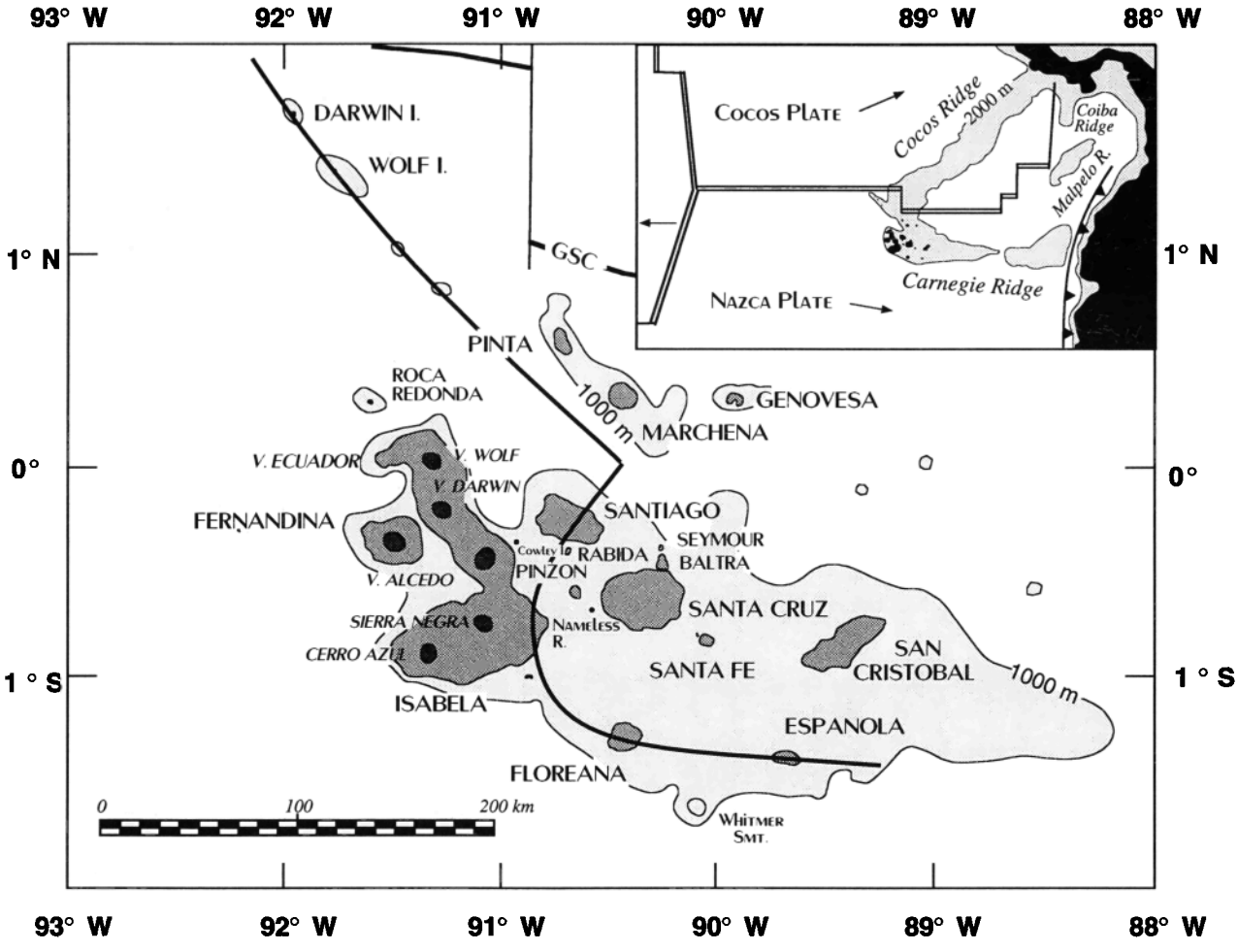

Fig. 1. Map of the Galápagos Archipelago. GSC is the Galápagos Spreading Center. Bold line shows the lithospheric fault system that separates thin, weak lithosphere to the north and east from stronger and thicker lithosphere to the south and west inferred by M. A. Feighner and M. A. Richards (submitted manuscript, 1993). Inset shows the regional tectonic setting.

GEOLOGICAL BACKGROUND AND PREVIOUS WORK

Tectonic Setting

The Galápagos Islands rise from a shallow submarine volcanic platform that is the western terminus of the east-west trending Carnegie Ridge. The Galápagos Spreading Center (GSC), which separates the Cocos plate from the Nazca plate and joins the East Pacific Rise in a triple junction some 1000 km west of the Galápagos Islands, bisects the region. The GSC is a moderately fast spreading ridge (~6 cm/yr) with significant asymmetric spreading over the last 5 m.y. along the section nearest the Galápagos (85° to 91°W) with more rapid spreading to the north [*Hey*, 1977]. Spreading elsewhere along this plate boundary has generally been symmetrical. North of Isabela Island, an ill-defined left-lateral transform fault at approximately 90°50'W offsets ridge segments by 150-km, and is the boundary between symmetric spreading ridge segments to the north and west, and the asymmetric segment to the south and east. This results in a 3-5 m.y. age difference in the lithosphere underlying the western and eastern halves of the archipelago.

The GSC has migrated northward away from the hotspot in the last 5-6 Ma, judging from the volcanic traces of the hotspot, the Cocos and Carnegie ridges [*Hey*, 1977]. Before that time, the hotspot lay directly beneath the GSC and contributed magmas concurrently to the production of the Cocos and Carnegie ridges, on the separating Cocos and Nazca plates, much as the Iceland hotspot generates paired volcanic ridges on the European and North American plates. With the northward migration of the ridge 5-6 m.y. ago, magma supply to the Cocos Ridge was essentially severed and the output of the hotspot focused on the western Carnegie Ridge. Dredging and Sea Beam studies of seamounts on the Carnegie Ridge revealed that at least some were once islands [*Christie et al.*, 1992], extending the time available for evolution of the unique Galápagos biota back to at least 9 Ma. The Coiba and Malpelo ridges are smaller blocks, dismembered from the eastern end of the Carnegie Ridge and transported northward during Nazca-South American plate collision [*Malfait and Dinkerman*, 1972; *van Andel et al.*, 1971]. Basement volcanic ages from these ridges support the hotspot model [*van Andel et al.*, 1973].

M. A. Feighner and M. A. Richards (Lithospheric structure and compensation mechaism of the Galápagos Archipelago, submitted to *Journal of Geophysical Research*, 1993) have analyzed gravity data from the Galápagos Platform and find that the center of the archipelago is underlain by weak lithosphere, with an elastic thickness of 6 km or less, and is close to Airy compensation. The western and southern portions of the platform are flexurally supported by a lithosphere with an effective elastic thickness of

about 12 km. The transition from strong to weak lithosphere appears to be abrupt and can be modeled as an arcuate fault that runs beneath Española and Floreana islands in the south, beneath easternmost Isabela in the west and intersects the Wolf Darwin Lineament, a northwest-southeast chain of small volcanos, of which only Wolf and Darwin Island rise above sea level, northeast of Santiago (Figure 1). The western boundary between strong and weak lithosphere essentially corresponds to an extention of the 90°50′W fracture zone, so that some of the difference in lithospheric strength may be attributable to the lithosphere to the west being 3-5 m.y. older than that to the east. Gravity modeling suggests the Wolf–Darwin Lineament may also be a lithospheric fault (M. A. Feighner and M. A. Richards, submitted manuscript, 1993). Seismicity also suggests a sharp contrast in lithospheric strength as the western part of the archipelago, including Fernandina and Isabela islands, is seismically active but very few earthquakes have been recorded from the central archipelago (M. A. Feighner and M. A. Richards, submitted manuscript, 1993). Based on gravity modeling, M. A. Feighner and M. A. Richards (submitted manuscript, 1993) find that crustal thickness increases from roughly 10 km on the margins of the platform to as much as 18 km beneath southeastern Isabela.

Two prominent structural lineaments control the alignment and spacing of islands rising from the Galápagos Platform [*Darwin*, 1860]. An east-west system parallels the Galápagos Spreading Center axis and the southern escarpment of the platform; it is most prominently expressed in block faulting on the islands of Baltra, Santa Cruz, and Santa Fe. A second, northwesterly system controls alignment of many of the Galápagos volcanos, particularly the large shield volcanos of Isabela as well as the Wolf-Darwin Lineament, extending from the platform to the GSC. Although both structural trends are seen on most central islands, east-west faults and fissures are best developed in the south central islands, whereas the northwesterly trend is most prominent west of the large transform fault offseting the GSC at 90°50′W. A symmetrical set of northeast trending fractures dominates the region east of another major transform fault at 86°W. The orientation of these oblique fractures at opposite ends of the offset ridge segment of the GSC bounded by two transform faults suggests that they result from the same forces responsible for the northward migration of the adjacent ridge segments (M. A. Feighner and M. A. Richards, submitted manuscript, 1993).

Geology of the Islands

The number of simultaneously active volcanos, their petrologic and morphological diversity, and the apparent lack of any simple evolutionary pattern all distinguish the Galápagos from more familiar examples of hotspot volcanism such as Hawaii. Charles Darwin made the first geologic observations of the islands in 1835 [*Darwin*, 1860]. The literature of the subsequent 150 years contains scattered reports on various aspects of the islands, but the first thorough geological study of the archipelago was that of *McBirney and Williams* [1969]. Subsequent studies [*Delaney et al.*, 1973; *Swanson et al.*, 1974; *Baitis*, 1976; *Lindstrom*, 1976; *Hall*, 1983; *McBirney et al.*, 1985; *Geist et al.*, 1985*a*, *b*; *Cullen and McBirney*, 1987; *Vicenzi et al.*, 1990; *Chadwick et al.*, 1991; *Chadwick and Howard*, 1991; *Rowland and Munro*, 1992; *Bow and Geist*, 1992; *McBirney*, 1993] have added considerable detail to our knowledge of the individual volcanos and islands.

Volcanos west of the 90°50′W fracture zone are distinct from the generally smaller and older eastern volcanos. The seven western volcanos of Isabela and Fernandina Islands are large, central shield volcanos with well-developed calderas, but they differ conspicuously from the familiar shields of Hawaii and Reunion [*McBirney and Williams*, 1969]. Their slopes steepen abruptly between a flat shelf close to sea level and a caldera rim, giving them a distinctive "inverted soup-bowl" outline. Eruptions occur either from circumferential fissures around the calderas, which are largely independent of the caldera-related normal faults, or from radial vents and fissures lower on the flanks [*Chadwick and Howard*, 1991]. *Simkin* [1984] argued that the unusual profile of the volcanos reflects the dominance of eruptions from the circumferential fissures. Alternatively, *Cullen et al.* [1987] proposed the profiles reflect growth of the volcanic through sill-like intrusions at 2-4 km depth below the summit. The differences in size and morphology between these volcanos and those east of the 90°50′ fracture zone probably reflects differences in lithospheric thickness. Thicker and older lithosphere west of the fracture zone can support larger volcanic structures (M. A. Feighner and M. A. Richards, submitted manuscript, 1993) and provides greater hydraulic head, allowing magma to ascend to greater height [*Vogt*, 1974].

Fernandina, at the extreme western edge of the platform, is the largest and apparently the youngest volcano in the archipelago. It has the deepest caldera (750 m) and the most frequent historic volcanic and seismic activity of any of the Galápagos volcanos. In 1968 the southeast portion of the caldera dropped by as much as 350 m in trap-door like fashion [*Simkin and Howard*, 1970]. In 1988, a large block of the eastern caldera failed and slid into the caldera. Oversteepening as a result of the 1968 caldera collapse and injection of a dike into the eastern caldera wall were probably responsible for this event [*Chadwick et al.*, 1991]. *Rowland and Munro* [1992] argue that this pattern, partial caldera floor collapse, followed by failure of the walls due to oversteepening, is typical of the growth of Fernandina caldera. They also concluded that at times in the past the caldera may have been filled, or nearly so, with ponded lavas. The present period appears to be one of low magma supply rate and caldera enlargement.

The island of Isabela is made up of five large shields and the truncated remains of a sixth, Volcan Ecuador. Most recent eruptions on Isabela have been centered on Sierra Negra and Cerro Azul at the southern end of the island. Volcan Wolf and Alcedo have erupted historically and despite a lack of reliable accounts of historic activity on Volcan Darwin, some of the lavas of that volcano are so fresh that they could well have been erupted within the last century or so. Volcan Alcedo, near the center of the island and directly downstream from the core of the hotspot, is mantled with rhyolitic pumice and the caldera contains a large flow of glassy rhyolite [*McBirney et al.*, 1985; D. J. Geist, manuscript in preparation, 1993]. Two smaller islands stand along the northern and southern extension of the main axis of Isabela. The steep-sided, flat-topped island of Roca Redonda is an eroded remnant of a lava-filled crater with active fumaroles that is about the same distance north of Volcan Wolf as the spacing of the shields on Isabela. In the opposite direction, Floreana Island and Wittmer Seamount lie along the same alignment.

The volcanos east of 90°50′W have more varied morphologies, eruptive histories, and compositions than the volcanos of Fernandina and Isabela. Floreana is a roughly circular, low shield whose outline is dominated by numerous parasitic cinder cones. *Bow* [1979] divided Floreana lavas into an older Main Series, comprising the shield-building lavas, and a younger Flank Series related to the pyroclastic eruptions that produced the cinder cones and the pyroclastic deposits that mantle much of the island. Paleomagnetic polarity measurements indicate that a substantial

part of the present shield existed prior to 0.78 Ma [*Cox and Dalrymple*, 1966]. Main Series lavas are primarily aphyric or sparsely olivine-phyric alkali basalts and basanitoids, often containing wehrlite, gabbro, and dunite xenoliths. Flank Series lavas, erupted from the parasitic cones that now decorate the island, are olivine- and plagioclase-phyric basanitoids that are somewhat poorer in alkalis and other incompatible elements than Main Series lavas [*Bow*, 1979; *Bow and Geist*, 1992]. Captain Porter of the U.S.S. *Essex* reported witnessing an eruption of Floreana in 1813, but it is possible he mistook Sierra Negra for Floreana [*Simkin et al.*, 1981]. As the Flank Series conformably overlies the Main Series, there is no evidence for a significant time gap between these two series. Because erosion rates in the Galápagos are generally low, however, such a gap is not precluded.

Santiago is a WNW elongate shield reaching an elevation of just over 900 m. The oldest lavas were erupted from summit vents in the central northwest highlands in an area now occupied by a faint caldera-like depression [*Swanson et al.*, 1974]. They range in composition from picritic alkali basalts through siliceous trachyte [*McBirney and Williams*, 1969; *Baitis*, 1976; *Swanson et al.*, 1974]. Somewhat younger lavas, again alkali basalts and their differentiation products, were erupted from east-west trending fissures in the central and eastern highlands. Olivine and plagioclase are the dominant phenocrysts in the basalts and are joined by augite in the more differentiated rocks [*Baitis*, 1976]. K-Ar ages reported by *Swanson et al.* [1974] range from 0.77 Ma to 0.14 Ma, and all lavas are normally polarized, implying ages less than 0.78 Ma. Recent activity has been concentrated at the northwestern and southeastern ends of the island and the southern flank and has produced a number of young tuff cones and islands, such as Bartholomé, just off the southeast end of the Santiago. These young flows, which are barren of vegetation and have perfectly preserved flow tops, cover about 25% of the island's surface. One flow in the James Bay area at the northwest end contains inclusions of quince marmalade jars stashed there by mariners and therefore must have been erupted within the 200 years preceding Darwin's mention of it during his 1835 visit. Several subsequent historic eruptions of olivine and plagioclase phyric basalts have occurred, the most recent in 1906.

Swanson et al. [1974] reported ages ranging from 0.92 to 1.09 Ma for Rábida and Pinzón. Rábida, near the south coast of Santiago, measures only 2.5 by 3 km and consists mainly of a cluster of steep-sided viscous domes, with the remains of two cinder cones at its northern base. Lavas range in composition from olivine tholeiite through ferrobasalt to dacite [*Swanson et al.*, 1974]. Pinzón is a small shield with two coalescing calderas. The high seacliffs on the southwestern side of the island expose at least seven eruptive cycles associated with the older, southern volcano [*Swanson et al.*, 1974]. Each begins with the explosive eruption of dacite or ferrobasalt (icelandite) followed by lavas of aphanitic ferrobasalt and finally plagioclase-rich tholeiite. The lavas in each sequence can be related by shallow fractional crystallization of the observed phenocrysts and may result from tapping successively deeper levels of a zoned magma chamber [*Baitis and Lindstrom*, 1980]. Activity subsequently shifted to the northern caldera, which erupted lavas and pyroclastics of similar composition.

Santa Cruz is a gently sloping, elliptical shield rising 950 m above sea level. A series of youthful pyroclastic cones and pit craters is aligned along a WNW trending axial fissure system defining the summit of the volcano. The island is cut by a number of east-west trending faults that are conspicuous along the northeastern, eastern, and southern coasts. The adjacent islands of Baltra and Seymour, to the north, and the Las Plazas islets, just off the east coast, are simple fault blocks.

Bow [1979] divided lavas of Santa Cruz into a Platform and Shield Series. The Platform Series is the older and occurs mainly in the northeast of the island; it constitutes all of Baltra, Seymour, and Las Plazas. The lowermost units of this series have morphologies indicative of submarine eruption and are intercalcated with shallow (< 100 m) marine carbonates. Windows of reversely polarized flows exposed at 300 m elevation on the northern slope of the shield are compositionally similar to flows exposed along the coast and are included in the Platform Series. Plagioclase with subordinate olivine dominates the phenocryst assemblage in Platform Series lavas, which are predominantly, though not exclusively, tholeiitic. A few of the plagioclase-ultraphyric lavas resemble the "abingtonites" of the northern islands [*Cullen et al.*, 1989]. Clinopyroxene is a phenocryst only in the differentiated ferrobasalts of Baltra and Seymour Islands.

Santa Cruz Shield Series lavas range from basanitoid to olivine tholeiite, but transitional alkali basalts predominate [*Bow*, 1979]. They are petrographically diverse and include olivine-only and plagioclase-dominant assemblages as well as aphyric lavas. The younger lavas included hawaiites. The youngest lavas, erupted from vents on the north slope as well as the summit fissure, are distinctly poor in K_2O and other incompatible elements. In places, these lavas uncomformably overlie the older platform series. According to *Bow* [1979], some flows appear to be no more than a few thousand years old judging from their morphology and lack of vegetation.

As the islands drifted eastward from the hotspot, they continued to have intermittent eruptions for at least 2 m.y. before finally becoming extinct. The island of San Cristobal at the far eastern end of the archipelago has the longest history of activity, having had at least five recognizable episodes of eruptions [*Geist et al.*, 1985*a*]. The southwestern half of the island is dominated by an older (2.35–0.6 Ma) shield volcano. The northeastern half consists primarily of relatively young basalts erupted from northeast-southwest fissures, though there are sparse outcrops of lavas erupted contemporaneously with the construction of the southwestern shield. Judging from the well-preserved flow top morphology and the sparse vegetation, the youngest of these lavas are certainly no more than a few thousand years old [*Geist et al.*, 1985*a*]. Petrologically, they are dominated by sparsely olivine- and plagioclase-phyric, relatively primitive (Mg# 60-70; Mg# is the atomic ratio of Mg to Mg + Fe^{2+}, expressed as percent) alkali basalts; tholeiites are much less common. Clinopyroxene phenocrysts occur only in the more evolved lavas, many of which contain gabbroic xenoliths. Though the lavas are compositionally heterogeneous, there is no systematic variation with age or location.

Santa Fe and Española are the only two major Galápagos islands that do not have volcanic morphologies. On the basis of brief visits, *McBirney and Williams* [1969] concluded both these islands were uplifted submarine platforms, but more detailed subsequent work shows that both consist predominantly of subareally erupted lavas [*Hall*, 1983; *Geist et al.*, 1985*b*]. Both have been disrupted by extensive east-west faulting. Though a number of small cinder cones, some related to the east-west faulting, have been identified on each, various indicators suggest that the main vent for Santa Fe lies offshore to the east [*Geist et al.*, 1985*b*] and that for Española lies offshore to the south [*Hall*, 1983]. Thus both are probably remnants of somewhat larger shields. The limited investigations to date suggest that Española lavas are relatively uniform and typically are primitive, olivine- and

plagioclase-phyric alkali basalts [*McBirney and Williams*, 1969; *Hall*, 1983]. Lavas from Santa Fe are typically transitional between alkali basalt and tholeiite and tend to be more evolved than those of Española [*Geist et al.*, 1985*b*]. Phenocrysts of olivine and plagioclase in the more mafic lavas are joined by augite in the more evolved rocks.

The northern islands form a distinct group. The two northernmost islands, Wolf and Darwin, are remnants of volcanos that rise 2000 m above the seafloor. Pinta, which last erupted in 1928 [*Simkin et al.*, 1981], is an elongated shield, bounded by a steep fault on its western side. *Cullen and McBirney* [1987] recognized an older shield, which emerged about 0.7 Ma, and a younger fissure stage. The compositional distinctions between these stages are subtle, both consisting of light-rare-earth-enriched olivine tholeiites. Marchena is a circular shield with a flooded caldera that last erupted in 1991. *Vicenzi et al.* [1990] recognized two lava series, separated by caldera formation and explosive activity. Both series consist predominantly of aphyric, moderately evolved tholeiites and alkali basalts, with little compositional distinction between the precaldera and postcaldera series. Genovesa is a smaller shield with a breached caldera, which forms Darwin Bay on the southern coast. The rocks have yet to be studied in detail, but reconnaissance sampling suggests comparatively uniform tholeiitic compositions. On the basis of well-preserved flow-top morphologies, the most recent eruptions probably occurred no more than a few thousand years ago. Mud in the bottom of saline Arcturus Lake, which fills a crater in the center of Genovesa, is less than 6000 years old [*Colinvaux*, 1984]. This also suggests Holocene volcanic activity on Genovesa. The most distinctive feature of the northern islands is the abundance of plagioclase-ultraphyric basalts (abingtonites), which can contain up to 40% percent large (≥ 1 cm) plagioclase phenocrysts [*Cullen et al.*, 1989].

With the notable exception of the northern islands, the distribution of rock types in the chain as a whole parallels the nearly east-west trend of the Carnegie Ridge. Petrographic variations are crudely symmetrical across the long axis of the platform with differentiated rocks concentrated in a belt along part of the east-west axis. Plagioclase is more common as a phenocryst in lavas from the center of the platform and less common on the southern islands and on Roca Redonda to the north. On the whole, however, the prevalence of plagioclase and the paucity of clinopyroxene phenocrysts in the more primitive lavas distinguishes the Galápagos from most other oceanic islands. For example, in basalt from the Makaopuhi lava lake on Hawaii, olivine crystallizes alone down to 7% MgO where it is joined by clinopyroxene and then by plagioclase at 1175°C [*Wright and Fiske,* 1971]. In contrast, crystallization of plagioclase always precedes clinopyroxene in Galápagos lavas, except in the most undersaturated basalts from Floreana, and it commonly occurs in lavas with over 8% MgO. This inferred paragenetic sequence has been confirmed by melting experiments of *Bow* [1979], which indicate that the first appearance of plagioclase occurs around 1190°C.

Analytical Methods

Samples collected during the initial reconnaissance study of the 1960s [*McBirney and Williams*, 1969] were analyzed by classical wet methods by K. Aoki in his laboratory at Scripps Institute of Oceanography. Samples collected during subsequent expeditions by McBirney and his students were analyzed by X ray fluorescence (XRF), atomic absorption, and neutron activation in laboratories at the University of Oregon for major and trace elements. Ferrous-ferric ratios were measured by titration and water contents by a DuPont moisture analyzer. Standards of the U.S. Geological Survey and the Geological Survey of Japan were used as controls throughout this period.

Because the quality of the early XRF analyses was found to be inferior to that of later ones performed by atomic absorption, many of the former were repeated by the latter method, and selected samples were analyzed by XRF by J. M. Rhodes at the University of Massachusetts. The same is true of instrumental neutron activation analysis (INAA), which also became more precise as improved methods were introduced. Thus all samples cited in the accompanying tables have been examined and revised to a uniform level of quality.

Isotopic data were acquired over a period of 15 years in three laboratories: the Department of Terrestrial Magnetism of Carnegie Institiution of Washington (DTM), the Max-Planck-Institut für Chemie (MPI), and the Department of Geological Sciences at Cornell University. Consequently, analytical procedures and the quality of the data vary somewhat. Chemical separation and mass spectrometry techniques used at DTM for Sr isotope and Nd isotope ratio measurements were those described by *Hart and Brooks* [1974] and *Whitford et al.* [1978]. These measurements were done on single collector mass spectrometers. Many of the older DTM data were reanalyzed at MPI and Cornell, and except as noted below, the reanalyses agreed within the older analytical error, once interlaboratory biases were taken into account. At MPI, Sr and Nd isotope measurements were carried out on Finnigan MAT261 mass spectrometers. Details of the procedures given by *White and Patchett* [1984]. Pb isotope ratios were determined using the technique described by *White and Dupré* [1986]. Cornell University data were acquired using a V.G. Sector mass spectrometer. At both MPI and Cornell, all samples were leached in hot 6 *N* HCl for 30-60 min prior to dissolution. Chemical separations were performed in the same manner as described by *White and Patchett* [1984]. After separation, Sr was loaded on single tungsten filaments with TaF_5 activator. Data were acquired using a dynamic triple collector technique, with each analysis consisting of 100-120 mass scans. Nd was loaded on triple filaments (Ta sides and Re centers) with a small amount of $H_2P_2O_4$ or on Re single filaments with $H_2P_2O_4$ and a small quantity of ion exchange resin [*Walker et al.*, 1989], which serves as a reducing agent. Data were acquired using a dynamic quadruple collector technique, each analysis consisting of 120-150 mass scans. Pb was separated using the technique described by *White and Dupré* [1986]. After separation, Pb was loaded on single Re filaments with silica gel, and data were acquired using a static quadruple collector technique. It differed from that described by *White and Dupré* [1986] only in that 80-100 ratio measurements were made rather than 60. A substantial fraction of the measurements were replicated; values reported here are averages of these replicates.

Rare earth elements, K, Rb, Cs, Sr, and Ba concentrations were determined by isotope dilution at DTM and at MPI. At DTM, light (Ce-Eu) and heavy (Gd-Yb) rare earth fractions were separated on an AG 50W-X8 ion exchange column and loaded on double Re filaments for isotopic analysis following a technique described by *Shimizu* [1974]. At MPI, the technique described by *White and Patchett* [1984] was employed for rare earth analysis. The two techniques differ in several respects. For the rare earths, the MPI technique used a second separation to isolate the rare earths into three fractions and included the analysis of La and Lu, which were not determined at DTM. In both laboratories, a

technique derived from that of *Hart and Brooks* [1974] was used for analysis of K, Rb, Cs, Sr, and Ba. The MPI technique corrected for mass fractionation for Sr, K, Cs, and Yb, whereas the DTM technique employed a mass fractionation correction only for Sr. This correction results in only a minor improvement in data quality. Estimated analytical uncertainties, based on replication of standards, range from 0.1% for Sm to 3.2% for Rb.

Trace elements were analyzed at Cornell by inductively coupled-plasma mass spectrometry (ICP-MS) using a V.G. Plasmaquad 2+ instrument. One hundred milligram samples were digested in HF and dried with $HClO_4$. They were then dissolved in 100 mL of 1% HNO_3. Ba and the rare earths were analyzed using an external calibration technique with drift correction [*Cheatham et al.*, 1993]. Rb, Sr, and Y were measured by standard addition. Estimated analytical uncertainties, based on replication of standards, range from 0.9% for Sr to 4.1% for Ba.

Radiometric ages were determined on whole rock samples by the K-Ar method. Rocks assessed to be unaltered on the basis of petrographic examination were crushed to 0.5-1.0 mm size fraction, ultrasonically washed in distilled water, and dried. A split of this cleaned, crushed fraction was removed and powdered for K analysis by atomic absorption spectrophotometry. Approximately 5 g of the crushed rock was loaded into a Mo-crucible for each argon analysis and a 1×10^{-8} torr vacuum was achieved by overnight baking (175°C) of the glass extraction line. Samples were then fused by radio frequency induction heating of the crucible, and active gases were gettered over a hot Ti-TiO_2 metal sponge. The isotopic composition of argon was then measured mass spectrometrically with an AEI MS-10S instrument at Oregon State University, connected on-line with the extraction system.

The majority of samples were analyzed in the conventional maner, introducing a known amount of ^{38}Ar spike during the fusion to determine the concentration of radiogenic ^{40}Ar [*Dalymple and Lanphere*, 1969]. For very young and low-K samples the analytical procedures of *Cassignol and Gillot* [1982] were adopted. This procedure yields improved precision for samples with low concentrations of radiogenic argon and is different in several ways. First, ^{38}Ar spike was not added because of small but significant amounts of ^{40}Ar and ^{36}Ar in the spike. Instead, sample ^{40}Ar concentration was determined from instrument sensitivity, which varied only 1-2% over long-term measurements of ^{38}Ar peak heights in spiked analyses and ^{40}Ar peak heights in atmospheric argon calibrations. Second, aliquots of air argon were routinely measured both before and after each sample analysis in order to make the important correction for atmospheric ^{40}Ar contamination as precisely as possible. This approach results in lower errors in correcting for atmospheric argon than spiking. Proportions of radiogenic ^{40}Ar as small as a few tenths of 1% of the total ^{40}Ar signal are thus detectable and reproducible [*Levi et al.*, 1990; *Gillot and Nativel*, 1989; *Prestvik and Duncan*, 1991].

RESULTS

Major Element Chemistry

Table 1 lists major element analyses and CIPW norms representative of the more primitive and more aphyric samples. (A complete table of 353 major element analyses used in this study is available on microfiche.[1]) Five oxides and CaO/Al_2O_3 are shown plotted against MgO in Figure 2. Figure 2 illustrates the wide range of compositions, much of which can be attributed to low-pressure fractional crystallization. Given the proximity of the islands to the Galápagos Spreading Center and the similarity in trace element and isotope geochemistry of many of the lavas to MORB, it seems appropriate to compare the major element chemistry to that of MORB, for which there is now a very extensive data base. The Galápagos data overlap the MORB fields extensively, but there are a number of subtle but important differences. First, though it is only partly apparent from Figure 2, the Galápagos data show somewhat more scatter about the fractional crystallization trends than MORB. Part of this is due to the Galápagos analyses being whole rock analyses while the MORB fields shown are for glass analyses. Some of the scatter therefore reflects accumulation of mineral phases (two obvious examples are the Al-rich lavas from Wolf Island; their Al-rich nature reflects plagioclase accumulation). Much of the scatter, however, seems to reflect greater variation in parental composition and the fractional crystallization process in the Galápagos. A second difference between the Galápagos and MORB is that Galápagos data extend to more MgO-rich compositions. A few of the MgO-rich samples are olivine cumulates, but others are aphyric or nearly so, and the whole rock analysis approximates the liquid composition. A third difference is the systematically lower SiO_2 concentration of the Galápagos lavas compared to MORB of similar MgO content. Figure 2 shows that at a given MgO concentration, the most SiO_2-rich Galápagos lavas have only the average SiO_2 concentration of MORB, while most have 1-2% less SiO_2 than is typical of MORB. Finally, the Galápagos lavas seem on average slightly richer in FeO, CaO, Na_2O, and Al_2O_3 than MORB at comparable MgO concentrations.

In Figure 3, two minor oxides, K_2O and TiO_2, are plotted against MgO; fields for MORB are shown for comparison. TiO_2 varies by a factor of 2 for a given MgO concentration in the Galápagos data; the variation in K_2O is even greater. Lavas from Genovesa, the northeasternmost island in the archipelago, generally have the lowest K_2O and TiO_2 for a given MgO concentration, while lavas from Floreana, the southeasternmost island, have the highest K_2O. Genovesa is actually poorer in K_2O than many MORB of comparable MgO content. While there is considerable overlap with the MORB field, the Galápagos lavas are on average richer in both K_2O and TiO_2 than MORB.

Figure 4 is two diagrams that have traditionally been used to discriminate alkali and tholeiitic basalts, and the Galápagos lavas are again compared to MORB. Figure 4a shows that though there is considerable scatter, the Galápagos lavas tend to cluster on the olivine-diopside join (the alkali basalt—tholeiite divide), while most MORB lie in the tholeiitic field in the center of the olivine-hypersthene-diopside field. Similarly, in the alkali-silica plot (Figure 4b) the Galápagos lavas scatter to both sides of the line that divides alkali basalts from tholeiites in Hawaii [*Macdonald and Katsura*, 1964]. As may be seen in Figure 4b, the Galápagos lavas are both poorer in SiO_2 and richer in alkalies than most MORB.

It is also useful to compare the chemistry of Galápagos magmas with those of Kilauea [*Wright and Fiske*, 1971], a more familiar and better understood example of oceanic island volcanism. At 8% MgO, only the lowest Na_2O concentrations in Galápagos lavas overlap those from Kilauea, and Galápagos lavas are systematically poorer in SiO_2 than ones. For the remaining oxides, the Galápagos range encompasses Kilauean values, but on average, the Galápagos are richer in Na_2O, CaO, and Al_2O_3 and poorer in TiO_2 and ΣFeO than Kilauean lavas at the same MgO concentration (8%). The higher Al_2O_3 concentrations in

[1]**Table of analyses is available with the entire article on microfiche. Order from American Geophysical Union, 2000 Florida Avenue, N.W., Washington, DC 20009. Document B93-005; $2.50. Payment must accompany order.**

TABLE 1. Representative Major Element Analyses and CIPW Norms of Galápagos Lavas

	G86-2 Espanola	G86-3 Espanola	E-41 Fernandina	FL-3 Floreana	E-134 Isabela Alcedo	E-152 Isabela Volcan Wolf	E-242 Isabela Volcan Darwin	E-56 Isabela Volcan Ecuador	CA89-2 Isabela Cerro Azul	SN-1 Isabela Sierra Negra
SiO_2	47.56	46.87	48.37	46.14	47.84	48.10	49.47	47.20	47.88	49.24
TiO_2	1.32	1.21	2.80	1.19	3.19	2.67	3.02	3.35	2.31	2.85
Al_2O_3	15.98	14.46	15.49	14.23	13.42	16.01	12.42	15.24	16.23	13.77
Fe_2O_3	5.01	2.12	2.75	2.09	6.97	3.45	3.85	3.50	3.34	2.32
FeO	5.13	7.17	8.59	7.06	6.14	7.20	8.70	8.42	7.24	10.70
MnO	0.22	0.18	0.18	0.18	0.10	0.17	0.19	0.17	0.16	0.21
MgO	8.48	12.79	6.72	12.59	6.21	6.32	6.24	6.37	6.37	5.58
CaO	10.08	10.68	11.60	10.51	11.56	11.48	11.27	10.45	12.48	10.30
Na_2O	3.37	2.60	2.77	2.56	2.63	2.87	2.97	3.11	2.81	3.10
K_2O	0.79	1.11	0.42	1.08	0.29	0.42	0.53	0.78	0.51	0.57
P_2O_5	0.40	0.81	0.05	1.10	0.21	0.32	0.31	0.40	0.28	0.42
H_2O^+	0.49		0.26	0.21	1.17	0.18	0.12	0.88	0.22	0.24
Total	98.83	100.00	100.00	98.94	99.73	99.19	99.09	99.87	99.83	99.30
						CIPW Norms				
ne	2.62	1.77		5.00				0.32	0.86	
or	4.70	2.71	2.48	6.52	1.76	2.52	3.18	4.70	3.01	3.41
ab	23.84	19.27	23.25	12.95	22.73	24.61	25.49	26.09	22.19	26.54
an	26.29	30.36	28.34	24.73	24.46	29.95	19.26	25.64	30.16	22.22
di	16.90	19.34	22.13	21.94	27.02	21.05	29.22	19.94	24.56	22.19
hy			6.19		10.81	5.20	10.42			12.57
ol	18.56	18.44	8.49	24.71	4.67	9.27	4.10	14.22	11.92	4.73
mt	3.02	3.05	3.19	1.33	1.84	1.51	1.79	1.70	1.65	1.88
il	2.52	3.65	5.28	2.32	6.20	5.15	5.83	6.46	4.39	5.49
ap	1.08	1.09	0.57	0.52	0.51	0.78	0.75	0.97	0.61	1.02
$Si_{8.0}$	48.10	47.10	48.05	48.56	47.00	47.73	49.12	46.50	48.71	48.46
$Fe_{8.0}$	9.12	9.63	9.53	9.82	10.25	8.42	10.22	9.62	10.93	10.00
$Na_{8.0}$	3.53	2.92	2.44	3.07	2.43	2.71	2.80	2.93	3.07	2.85
$K_{8.0}$	0.83	0.53	0.33	1.29	0.19	0.33	0.44	0.69	0.66	0.44
Mg #	61.1	64.7	54.6	71.5	47.1	52.2	47.8	49.5	52.6	43.8

	E-169 Genovesa	M-34 Marchena	P-42 Pinta	PS-16 Pinzon	E-165 Rabida	SC-61 San Cristobal	SC-75 San Cristobal	E-1 Santa Cruz	G86-1 Santa Cruz	SC-196 Santa Cruz	SC-78 Santa Cruz
SiO_2	48.65	49.00	49.71	47.85	48.87	47.72	47.42	46.14	47.14	48.56	46.44
TiO_2	1.36	2.67	2.41	1.78	0.69	1.41	1.08	2.01	1.87	2.61	1.03
Al_2O_3	16.25	14.57	15.30	15.79	17.72	16.74	16.86	16.10	15.67	14.76	15.92
Fe_2O_3	3.03	3.50	2.14	6.13	2.35	2.08	1.32	2.26	3.70	2.20	1.58
FeO	7.57	9.34	8.64	5.05	5.20	6.61	7.38	9.07	7.70	11.04	9.31
MnO	0.18	0.21	0.18	0.19	0.12	0.17	0.17	0.19	0.20	0.23	0.19
MgO	8.09	5.78	6.41	7.89	8.73	9.73	11.62	10.43	8.62	6.98	12.36
CaO	12.01	10.85	11.21	11.37	12.21	12.12	11.84	9.19	10.42	10.69	10.73
Na_2O	2.64	3.43	3.13	2.56	2.74	2.53	2.06	3.64	2.94	3.20	2.28
K_2O	0.11	0.35	0.74	0.27	0.17	0.49	0.18	0.26	0.35	0.35	0.08
P_2O_5	0.10	0.13	0.36	0.28	0.14	0.19	0.10	0.24	0.26	0.26	0.08
H_2O^+	0.01	0.30	0.05	0.23	0.21	0.22	0.17	0.48	0.54		
Total	100.01	100.13	100.3	99.39	99.15	100.00	100.20	100.01	99.41	100.88	100.00
						CIPW Norms					
ne	1.54					1.58		5.05	0.39		0.57
or	0.30	2.07	4.37	1.62	1.02	2.88	1.06	1.54	2.10	2.04	0.50
ab	19.32	29.02	26.49	21.98	23.48	18.62	17.44	21.68	24.54	26.89	18.24
an	31.58	23.33	25.51	31.24	36.00	33.00	36.25	27.00	28.95	24.71	33.01
di	27.90	23.73	22.79	19.76	19.77	21.13	17.64	14.08	17.82	21.72	15.99
hy		2.04	3.59	6.99	0.76		2.28			1.24	
ol	15.28	11.84	10.27	12.77	16.22	18.44	21.78	24.61	20.36	15.99	27.98
mt	1.44	2.01	1.70	1.55	1.07	1.24	1.24	1.62	1.62	1.88	1.56
il	2.42	5.07	4.58	3.44	1.33	2.69	2.06	3.85	3.61	4.93	1.96
ap	0.24	0.63	0.79	0.68	0.34	0.45	0.24	0.58	0.63	0.62	0.20
$Si_{8.0}$	48.71	47.61	48.72	48.11	49.21	48.55	48.78	47.17	48.02	48.55	48.02
$Fe_{8.0}$	10.35	10.98	9.49	10.56	8.20	9.17	9.29	11.80	11.55	12.33	11.46
$Na_{8.0}$	2.66	2.96	2.79	2.57	2.82	2.80	2.45	3.95	3.10	2.98	2.72
$K_{8.0}$	0.11	0.32	0.72	0.27	0.21	0.63	0.35	0.42	0.36	0.34	0.26
Mg #	59.9	45.2	52.0	57.1	68.0	67.2	70.7	62.6	58.2	48.9	67.2

	G86-5 Santa Fe	SF-13 Santa Fe	BL-1 Santiago	JH-86 Santiago	SH-7 Santiago	W90-4 Wolf Island	DA-2 Darwin Island	E87-3 Cowley Island	E-156 Roco Redonda
SiO_2	47.77	46.72	47.94	46.46	47.26	49.09	49.91	47.30	44.19
TiO_2	2.99	1.90	1.27	1.26	2.42	1.13	1.52	2.61	2.21
Al_2O_3	15.12	15.60	16.53	16.00	15.40	15.23	15.26	14.28	11.45
Fe_2O_3	6.77	3.41	4.17	2.95	3.17	6.09	7.45	3.24	3.21
FeO	5.03	7.69	6.15	7.37	9.38	5.25	2.74	9.19	9.69
MnO	0.19	0.18	0.17	0.18	0.21	0.18	0.19	0.17	0.19
MgO	5.59	9.69	9.34	10.79	7.58	6.50	7.30	7.83	16.98
CaO	9.12	10.23	11.76	11.97	11.26	12.19	12.40	10.18	7.47

TABLE 1. (continued)

	G86-5 Santa Fe	SF-13 Santa Fe	BL-1 Santiago	JH-86 Santiago	SH-7 Santiago	W90-4 Wolf Island	DA-2 Darwin Island	E87-3 Cowley Island	E-156 Roco Redonda
Na_2O	3.51	3.03	2.64	2.28	3.24	2.95	2.90	3.07	2.32
K_2O	1.03	0.55	0.10	0.06	0.31	0.29	0.32	0.45	0.64
P_2O_5	0.77	0.35	0.18	0.10	0.27	0.48	0.20	0.26	0.32
H_2O^+	1.40	0.10	0.09	0.27		0.23	0.22	0.04	0.67
Total	99.29	99.45	100.34	99.69	100.50	99.61	100.41	98.62	99.34
					CIPW Norms				
ne		2.49		1.04	2.79				1.85
or	6.09	3.28	0.59	0.36	1.83	1.14	1.71	2.71	3.87
ab	29.70	21.29	22.37	17.54	22.21	21.11	24.96	26.43	16.55
an	22.46	27.60	33.00	33.52	26.50	51.50	27.46	24.27	19.24
di	14.65	17.36	19.74	20.85	22.61	14.84	24.67	20.84	13.13
hy	3.34		0.12			1.97	3.68	0.32	
ol	11.85	21.92	19.90	22.56	17.07	5.84	11.42	17.98	38.50
mt	1.79	1.58	1.44	1.47	1.77	0.89	1.73	1.79	1.85
il	5.68	3.65	2.42	2.42	4.60	2.16	2.15	5.05	4.27
ap	1.68	0.85	0.43	0.24	0.65	0.55	1.05	0.63	0.78
$Si_{8.0}$	48.13	47.81	48.66	47.59	47.47	48.15	49.47	47.59	47.07
$Fe_{8.0}$	9.75	11.51	10.59	10.73	11.95	9.71	8.97	12.77	13.38
$Na_{8.0}$	3.08	3.31	2.87	2.61	3.15	2.63	2.75	3.20	3.08
$K_{8.0}$	1.02	0.70	0.24	0.22	0.30	0.27	0.31	0.58	0.87
Mg #	47.3	61.6	62.7	65.7	52.5	51.9	58.0	53.6	70.6

Mg# = $(Mg^{2+}/(Mg^{2+}+Fe^{2+}))_{atomic}$ and norms calculated assuming ferric iron is 10% of total iron. E-1 is from *McBirney and Williams* [1969]; PS-16, JH-86, and SH-7 are from *Baitis* [1976]; FL-3, SC-78, and *SC-196* are from *Bow* [1979]; SC-61 and SC-75 are from *Geist et al.* [1985*a*], M-34 is from *Vicenzi* [1985], P-42 is from *Cullen* [1985]. See text for an explanation of $Si_{8.0}$, etc. A complete table of 353 major element analyses used in this study is available on microfiche. These data, as well as data in Tables 3 and 5 are also available upon request as Microsoft Excel® files on floppy disk from W. M. White.

Galápagos lavas explain the early appearance and predominance of plagioclase discussed earlier.

Figures 2-4 illustrate the contrasts in compositional variability in Galápagos volcanos. Data from the large western volcanos on Isabela and Fernandina, as well as Pinta and Marchena, form reasonably tight clusters on these diagrams. These volcanos have erupted only fractionated basalt of a limited compositional range, with MgO generally in the range of 4–7%. Alcedo is somewhat of an exception as it has erupted differentiation products which range through rhyolite. Basalts from Genovesa, though less differentiated, also have a fairly restricted range (8.5–6% MgO) and form reasonably coherent trends on MgO variation diagrams. The two northernmost islands, Darwin and Wolf, also seem compositionally uniform, once the effects of plagioclase accumulation are discounted, but sampling of these volcanos is less complete. In contrast, the products of the remaining volcanos, most notably Santa Cruz, San Cristobal, Santiago, Santa Fe, and Floreana, are distinctly more heterogeneous both in MgO and in the value of other oxides at a given MgO content. Española seems to fall into the latter group, in contrast to the conclusion of *Hall* [1983] that Española magmas are relatively homogeneous, but our data for that island are limited. A range of parental magma compositions is required on each of these islands.

Lavas more differentiated than basalt are found only in the central belt extending east from Alcedo Volcano on Isabela. The rhyolites of Alcedo, near the center of Isabela, are the most extreme volcanic differentiates, but Pinzón and Rábida, a short distance downstream (east), consist predominantly of ferrobasalts, icelandites, and dacites with lesser amounts of siliceous trachyte. The adjacent island of Santiago has a mildly alkaline series of hawaiites, mugearities, and trachytes. Ferrobasalts and hawaiites also occur on Santa Cruz, just to the east. Plutonic xenoliths have been ejected from explosive vents on all islands on this central axis, but the most differentiated rocks, including ferrogabbro, ferrodiorite, and quartz syenite, are found in a small cinder cone on the northern coast of Rábida island. Their compositions are equivalent to those of the differentiated tholeiitic lavas. This restriction of strongly differentiated magmas to the center of the archipelago is part of a more general geographic pattern in which the minimum observed Mg concentration or Mg# decreases toward the center of the archipelago.

Geochronology

Table 2 lists new K-Ar age determinations for rocks analyzed in this study. In Figure 5 most of these ages are plotted against distance from Fernandina, presumed to be the leading edge of the hotspot, in the direction of motion of the Nazca plate (100.5° [*Gripp and Gordon*, 1990]). Ages from Wolf and Darwin Islands are not plotted, as these volcanos lie "upstream" from the hotspot and cannot be related to the remainder of the islands by plate motion alone. Also plotted are the previously measured K-Ar ages from the islands [*Cox and Dalrymple*, 1966; *Swanson et al.*, 1974; *Bailey*, 1976], recalculated to currently accepted decay and abundance constants (see Table 2). The two sets of age determinations overlap completely, although analytical uncertainties for the earlier measurements are often much larger than for the new age determinations; the two oldest ages reported (Santa Cruz: 4.2 ±1.8 and 3.8 ± 1.8 Ma [*Bailey*, 1976]) are not plotted because of their imprecision. Likewise, a previously reported age for Santa Fe (3.9 ± 0.6 Ma, *Geist et al.* [1985*b*]) had a large analytical uncertainty and was remeasured at 2.50 ± 0.08 Ma (sample SF-13, Table 2). The two analyses do not agree within experimental error; the second analysis is preferred because a much larger proportion of radiogenic ^{40}Ar was measured.

While, in general, the age of Galápagos volcanism shows little relationship to distance, the ages of the oldest flows at each of the islands form a reasonable progression from youngest in the west to oldest in the east. The oldest flows on a volcano are likely to be buried by subsequent activity, so our dates certainly overrepresent the younger flows. Given this sampling bias, the geochronological data are entirely consistent with the simple model of inception of

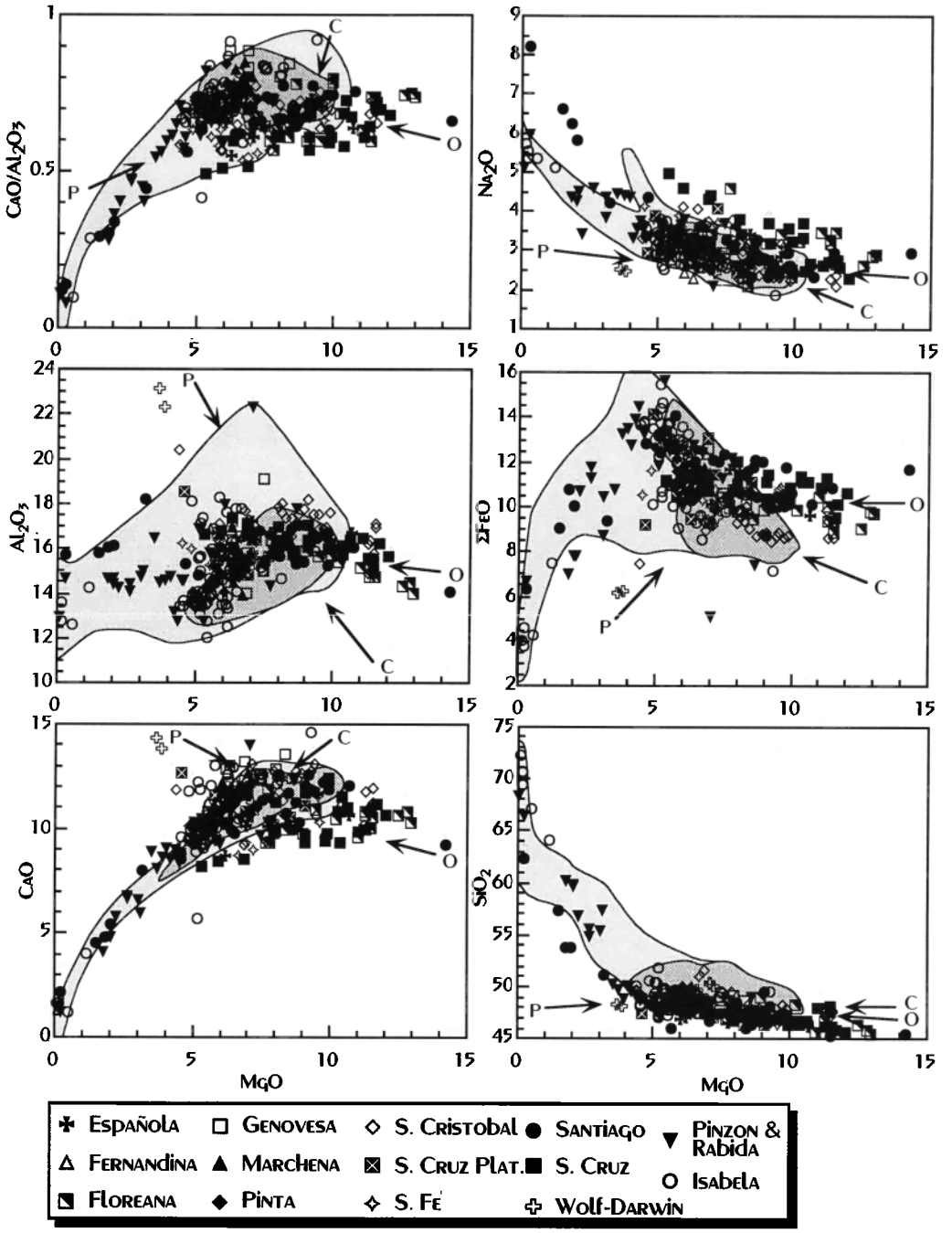

Fig. 2. Variation of major oxides as a function of MgO in Galápagos lavas. Light and dark shaded areas enclose 99% and 95%, respectively, of 1000 analyses of MORB from the East Pacific Rise. Lavas from Baltra, Seymour, and Las Plazas Islands are grouped in this and subsequent figures with the Santa Cruz Platform Series. Similarly, Roca Redonda is grouped with Isabela, and Cowley Island and Nameless Rock are grouped with Pinzón and Rábida.

volcanism on a plate moving over a stationary mantle plume. A second feature of Galápagos volcanism apparent from Figure 5 is the extensive period over which volcanism has occurred on several islands. Volcanism has continued on San Cristobal for a period of over 2.4 m.y., and extended over a period of at least 2 m.y. on Santa Fe. Santa Cruz, Pinta, and Floreana all have been active for periods of nearly a million years and more. Clearly, most of the dated flows erupted at locations well to the east of the leading edge of the hotspot, indicating either an extended zone of melting "downstream" from the plume or postshield extensional volcanism across the platform region that allowed asthenospheric melts to reach the surface through old shield volcanos.

Contamination of Isotope Ratios in Subaereal Oceanic Basalts

Table 3 reports isotope ratios. During the course of this study, we found in a few cases that leaching samples in hot 6 *N* HCl before dissolution lowered Sr isotope ratios significantly. Table 4 compares $^{87}Sr/^{86}Sr$ ratios of leached and unleached analyses for those cases where significant differences were found. In a few cases, such as SC-196 and E-111, the samples showed some evidence of weathering and alteration. These samples may have been submerged during high stands of sealevel in the past, where they would have been exposed to seawater. Leaching probably removed Sr of seawater derivation in secondary phases in these

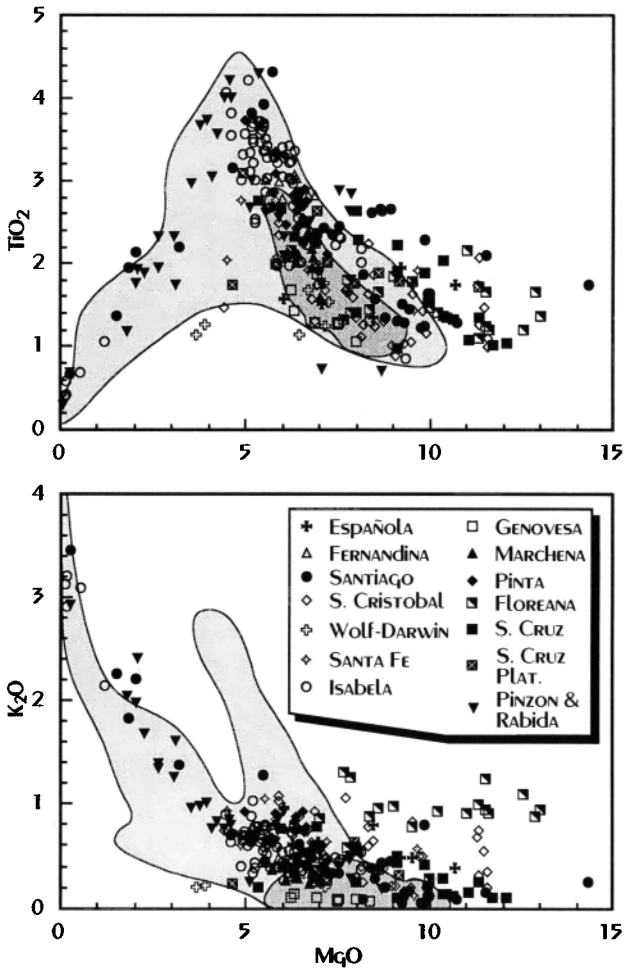

Fig. 3. Variation of minor oxides K_2O and TiO_2 with MgO in Galápagos lavas. Shaded regions are the fields for MORB as in Figure 2.

cases. However, in most of the other samples whose $^{87}Sr/^{86}Sr$ decreased after leaching, there was no visible evidence of alteration or weathering. Indeed, most appear quite young and were undoubtedly never directly exposed to seawater. A similar phenomenon was observed during reanalysis of samples from Easter Island (original data reported by *White and Hofmann* [1982]): $^{87}Sr/^{86}Sr$ of leached samples were systematically 0.0002 to 0.0003 lower than from unleached samples., and *S. R. Hart* [personal communication, 1992] has observed the same phenomenon with young basalts from the Reykjanes Peninsula of Iceland.

For the young, apparently unaltered basalts, the origin of the relatively radiogenic Sr removed by leaching is not obvious. On oceanic islands composed entirely of young basalt, seawater is the only source of radiogenic Sr. We suggest that the seawater contaminant is delivered as an aerosol derived from breaking waves. This seawater mist is deposited on the rocks, where the water would evaporate, leaving a residue of sea salt. Seawater contains only 8 ppm Sr, much less than the basalts, but sea salt contains 230 ppm Sr, a concentration comparable to that in the rocks. The concentration of Sr in the residual salt may well be enhanced if the rocks are washed by rainwater. Sr in sea salt may be largely held in calcite, which would dissolve much more slowly in rainwater than halite, the principal phase in sea salt. Repeated cycles of deposition of sea salt and washing by rain over thousands of years could leave a residue consisting of calcite, gypsum, and other relatively insoluble minerals in which the concentration of Sr might exceed 1000 ppm. The presence of amounts of this salt too small to notice could still shift Sr isotope ratios significantly. For example, if the salt contained 1000 ppm Sr with $^{87}Sr/^{86}Sr = 0.7092$, about 2% of it would be required to produced the isotopic shift observed in sample E-4. The substantial chloride content of rainwater [e.g., *Brown et al.*, 1989] suggests contamination of Sr isotope ratios by this mechanism may be a problem even 100 to 150 km from coasts.

Another potential source of seawater Sr contamination is guano. This appears to be a problem for sample WO-1, a vesicular lava from Wolf Island with guano in the vesicles. Its $^{87}Sr/^{86}Sr$ is significantly higher than ratios from other samples from Wolf and Darwin Islands as well as dredged samples from the Wolf-Darwin Lineament [*Harpp et al.*, 1990], though its ε_{Nd} and Pb isotope ratios are similar. This suggests that our leaching procedure failed to remove all the guano.

Sample E87-1 is a lava bomb in palagonite tuff from Nameless Rock, a small tuff ring remnant now only several tens of meters in diameter. The sample was collected from within a few meters of sea level and shows obvious signs of alteration. Its extremely high $^{87}Sr/^{86}Sr$ (0.70714) suggests that significant amounts of seawater-derived Sr remained after leaching. Because we suspect contamination for both WO-1 and E87-1, the Sr isotope ratios of these samples are not plotted in any of the figures or considered in our subsequent discussion.

Whatever the source of the contamination, it appears that leaching in hot HCl before Sr isotope ratio analysis is advisable even for apparently fresh basalts. If the contaminant Sr is either residual sea salt or guano, washing in distilled water might not be sufficient to remove Sr-bearing compounds having only limited solubility.

Isotope Ratios

Sr and Nd isotope ratios plotted in Figure 6 reveal a range of isotopic compositions between those typical of MORB and values near the median of the oceanic island basalts. Most of this variation occurs between volcanos. Individual volcanos or islands are more homogeneous than the data set as a whole, but significant variations nevertheless occur between lavas of individual volcanos on some islands, e.g., Floreana, San Cristobal, and Pinta. In other cases, such as Española and Fernandina, the eruptive products of the volcanos appear virtually homogeneous within analytical error. Though this may reflect the limited sampling in some cases, in others, e.g., Marchena, an island for which we have an extensive data set, variability is still quite limited, indicating that Galápagos volcanos can be nearly isotopically homogeneous. In general, those volcanos whose eruptive products have limited ranges of major element composition are also isotopically homogeneous, while those with a greater range in major element composition are isotopically heterogeneous. Thus most of the large western volcanos are isotopically homogeneous. Volcan Ecuador and Volcan Alcedo are exceptions, as their lavas exhibit significant isotopic heterogeneity. The Alcedo rhyolite, E-135, has isotope ratios in the middle of the range for the Alcedo basalts, consistent with its evolution by fractional crystallization from a basaltic parent.

Floreana, Santa Cruz, San Cristobal, Santa Fe, and Santiago all exhibit a significant range in isotope ratios. The variation in

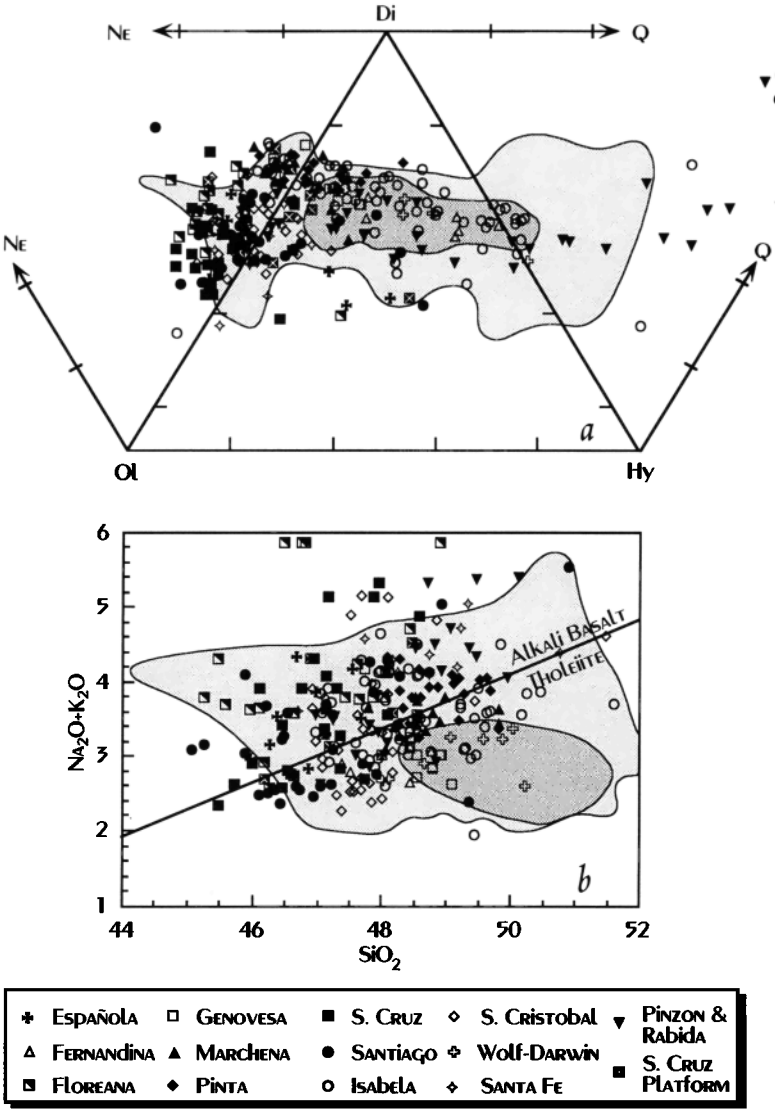

Fig. 4. (a) Exploded view of the normative basaltic tetrahedron projected from plagioclase [*Yoder and Tilley*, 1962], and (b) alkali-silica diagram. Norms were computed assuming ferric iron is 10% of total iron. Shaded region are the fields for MORB as in Figure 2. Line dividing Hawaiian alkali basalts from tholeiites [*Macdonald and Katura*, 1964] is shown for comparison.

Santiago is largely geographic: basalts from the southeast have distinctly more depleted isotopic signatures than those from the northwest. Within each subset, there is no systematic variation with age: the older lavas have similar isotope ratios to the historic flows in that part of the island. This suggests that Santiago may consist of two coalesced volcanos, a southeastern one and a northwestern one, which have been fed by distinct mantle sources throughout their histories. This situation is reminiscent of the Hawaiian volcanos. The variation in Santa Cruz (including the adjacent small islands of Baltra, Seymour, and Las Plazas) is also geographic, but this variation is probably fundamentally temporal: the Platform Series lavas of the northeast are about 1 m.y. old, while the remainder of the island, composed of the Shield Series, is younger. In San Cristobal, there is no clear relationship of isotope ratios to age or location. On Floreana, the variation also appears unrelated to age or location: ranges for the Main and Flank Series overlap almost completely.

The correlation between Sr and Nd isotope ratios is somewhat better than reported by *White and Hofmann* [1978], a result of the removal of contaminant seawater Sr by leaching as described above, but it remains imperfect. For example, Floreana samples have systematically higher $^{87}Sr/^{86}Sr$ than Pinta, even though the $^{143}Nd/^{144}Nd$ ratios of the two are comparable. Samples from the two southern volcanos on Isabela Island, Cerro Azul and Sierra Negra, plot between Pinta and Floreana.

Figure 7 shows Pb isotope ratios. The data cover a substantial part of the oceanic basalt range, with $^{206}Pb/^{204}Pb$ varying from 18.4 to 20.0. As with Sr and Nd isotope ratios, most of this variation is between, rather than within, volcanos. Though a strong overall correlation exists among the three Pb isotope ratios, individual islands or volcanos can deviate from this correlation. For example, samples from Darwin, Wolf, and Pinta islands have somewhat high $^{207}Pb/^{204}Pb$ and $^{208}Pb/^{204}Pb$ for a given $^{206}Pb/^{204}Pb$ ratio when compared to the other islands.

The relationships between Pb and Sr and Nd isotope ratios are shown in Figure 8. Pb isotope ratios show a strong positive correlation with $^{87}Sr/^{86}Sr$ and a strong inverse one with ε_{Nd}. As in the previous figures, individual islands and volcanos tend to exhibit better correlations than the entire data set.

The overlap of the Galápagos data with the MORB field is

TABLE 2. K-Ar Age Determinations on Galápagos Basalts

Sample	Location	Percent K	Percent Radiogenic ^{40}Ar	Age ±1σ, Ma
Espanola				
G86-2	Gardner Bay	0.645	3.08	2.61±0.15
G86-3	Punta Suarez	0.391	24.18	2.77±0.04
Floreana				
FL-3	Main Series	0.894	3.66	1.52±0.08
E-110	Flank Series	0.365	0.12	0.08±0.13
E-108	Flank Series	0.365	0.72	0.35±0.11
Genovesa				
G86-8		0.072	0.00	0.00
Isabela				
E-237	Volcan Darwin	0.582	0.00	0.00
E-142	Volcan Alcedo	2.440	7.88	0.15±0.02
			6.97	0.12±0.01
DG-48	Volcan Alcedo	2.930	3.90	0.074±0.024
DG-43	Volcan Alcedo	0.430	0.00	0.00
DG-27	Volcan Alcedo	0.450	0.52	0.15±0.05
Marchena				
E-10		0.172	0.88	0.10±0.04
M-34		0.299	4.69	0.56±0.04
M-51		0.241	1.42	0.11±0.02
M-67		0.176	0.73	0.12±0.04
M10		0.172	0.88	0.10±0.04
Pinta				
E-8		0.627	0.28	0.036±0.025
P-21		0.357	2.81	0.89±0.24
P-50		0.400	0.00	0.00
Pinzón				
E-68b		0.504	3.24	1.40±0.08
E-70		1.20	3.04	1.04±0.07
San Cristobal				
SC-5	Southwest	0.838	1.43	0.77±0.18
SC-20	Southwest	0.888	6.82	1.33±0.04
SC-23	Southwest	0.473	33.27	2.35±0.03
SC-28	Southwest	0.639	15.36	0.89±0.03
SC-34	Southwest	0.539	21.04	2.33±0.039
SC-61	Northeast	0.540	0.27	0.050±0.039
Santa Cruz				
G86-1	Las Plazas	0.271	3.67	1.31±0.10
SC-108	NE Platform	0.573	6.26	1.12±0.07
SC-151	South Shield	0.662	0.31	0.03±0.025
			1.19	0.024±0.011
Santa Fe				
G86-4		0.516	16.57	2.76±0.04
G86-5		0.800	1.35	0.72±0.09
SF-13		0.515	7.27	2.50±0.08
Darwin Island				
DA-1		0.303	0.45	0.39±0.15
DA-2		0.266	0.48	0.41±0.16
Wolf Island				
W90-2		0.249	4.92	1.60±0.07
W90-4		0.241	3.97	0.88±0.13
Roco Redonda				
E-156		0.534	0.19	0.053±0.054

Ages calculated using the following decay and abundance constants: $\lambda_e = 0.581 \times 10^{-10}\ yr^{-1}$; $\lambda_\beta = 4.962 \times 10^{-10}\ yr^{-1}$; $^{40}K/K = 1.167 \times 10^{-4}$ mol/mol.

particularly noteworthy. Although *Zindler et al.* [1979] also reported relatively low $^{87}Sr/^{86}Sr$ and high $^{143}Nd/^{144}Nd$ for Iceland, the data reported here, particularly those for the Genovesa and some of the Santa Cruz basalts, are the lowest $^{87}Sr/^{86}Sr$ and highest $^{143}Nd/^{144}Nd$ yet found on oceanic islands. Pb isotope ratios from these islands also overlap the MORB fields.

Trace Elements

Table 5 reports concentrations of rare earths and other trace elements. Chondrite-normalized rare earth element (REE) patterns are shown in Figures 9-12. A remarkable variation in rare earth patterns is apparent, ranging from fairly strongly light rare earth element (LREE) enriched basalts from Floreana to the LREE-depleted basalts of Genovesa. Only moderately to strongly LREE-enriched lavas have been observed on Floreana, Pinta, Española, Isabela, and Fernandina. The Marchena basalts are slightly concave downward, with a maximum at Nd or Sm; that is, the lightest rare earths are depleted relative to the intermediate rare earths but enriched relative to the heavy REE. Only LREE-depleted lavas occur on Genovesa, while both LREE-enriched and LREE-depleted lavas occur on Santiago, Santa Cruz, Santa Fe, and San Cristobal. These latter four islands also show the greatest diversity in major element chemistry and isotope ratios. The rare earth patterns of the large western volcanos of Fernandina and Isabela are particularly uniform, as are their major element chemistry and isotope ratios. The rare earth patterns of the seven basalts analyzed from Volcan Darwin are all essentially parallel, though the absolute abundances vary by a factor of nearly three between E-217 and E-224. The patterns of the two basalts analyzed from Fernandina are virtually indistinguishable. Thus the same contrasts in compositional diversity observed for major elements and isotopes also extend to the rare earths.

The REE patterns in Genovesa basalts, and some basalts from Santiago and Santa Cruz, are noteworthy in that they are indistinguishable from those of typical MORB. The concentrations of K, Rb, Cs, and Ba in the Genovesa basalts, as well as some of the Santa Cruz shield (e.g., SC-78, SC-100) and Santiago (e.g., SH-75a) basalts, are very low, and are also well within the range of typical MORB. Sr concentrations are slightly higher than that of average normal MORB (N-MORB), which in some cases could be a result of plagioclase accumulation as some of these lavas are plagioclase-rich. Thus in all their trace element and isotopic characteristics, a number of basalts from the center of the Galápagos Archipelago are virtually indistinguishable from N-MORB, a feature that appears to be unique to the Galápagos.

As expected, there is a general correlation between trace element abundances and isotope ratios. Thus Floreana, Pinta, and the southern Isabela volcanos, which have the most enriched isotopic signatures, are all LREE-enriched, while Genovesa basalts, with a depleted isotopic signature, are LREE-depleted. In detail, however, this correlation is very imperfect. For example, although basalts of Volcan Darwin and Volcan Wolf both have fairly depleted isotopic signatures, they are LREE-enriched. More surprisingly, some of the Santa Cruz basalts with MORB-like isotope ratios are LREE-enriched.

Among the LREE-enriched basalts there is a subtle difference in patterns. All LREE-enriched lavas with depleted isotopic signatures have concave-downward LREE patterns, that is, they flatten toward La. Lavas with less depleted isotopic signatures have straight or concave-upward light rare earth patterns. A good example of this difference can be seen in Figure 9, where the concave-downward patterns of Volcan Wolf lavas, which have $\varepsilon_{Nd} \sim +8$, contrast with the straight patterns of lavas from Volcan Ecuador, which lies only 10 km to the east, and Roca Redonda to the north, both of which have $\varepsilon_{Nd} \sim 6.5$.

There is also a systematic variation in heavy rare earth patterns. Among the LREE-enriched basalts, those from the southern part of the archipelago, most notably basalts of Floreana, Española, and San Cristobal, have comparatively flat heavy rare earth (Gd-Lu) patterns, while LREE-enriched basalts from the remainder of the archipelago generally have inclined heavy rare earth patterns. This difference is most easily seen when the rare earth patterns of Floreana or Española are compared with those of Rábida or Pinzón in Figure 10.

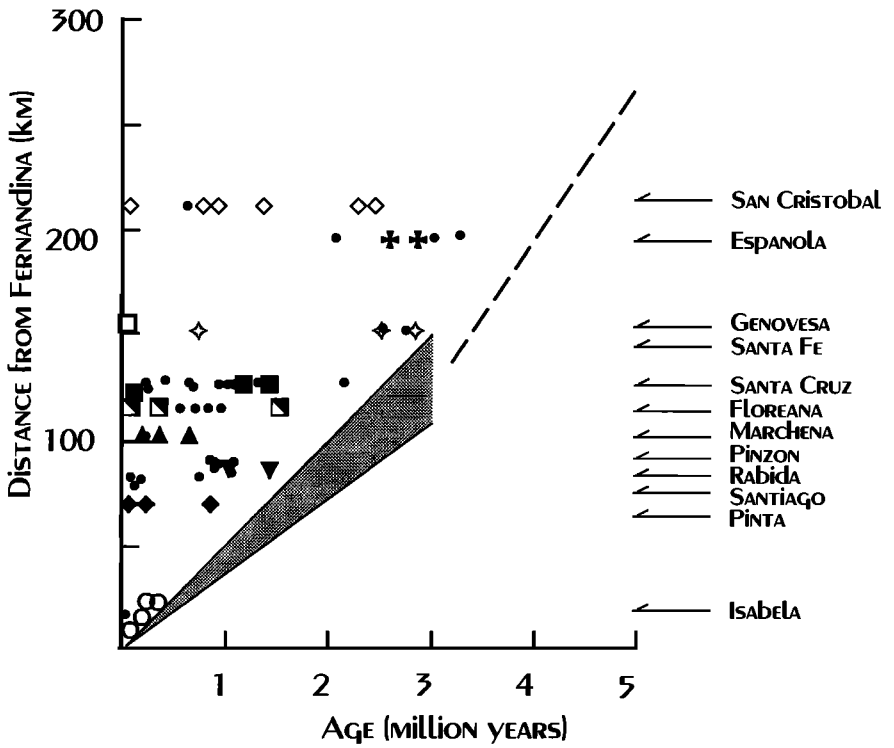

Fig. 5. Present distance of Galápagos lavas from the westernmost eruptive center (Fernandina) plotted against their K-Ar ages. Shaded region shows the position predicted from 37 mm/yr motion of the Nazca plate [*Gripp and Gordon*, 1990] over a fixed hotspot centered beneath Fernandina. Small dots are data from the literature; larger symbols are from Table 2. Dashed line illustrates the pre-3 Ma motion of 65 mm/yr [*Minster and Jordan*, 1978].

Relationships Among Major Elements, Trace Rlements, and Isotope Ratios

Because fractional crystallization can obscure compositional relationships that might, in primitive rocks, elucidate variations in source composition, depth of melting, and degree of melting, *Klein and Langmuir* [1987] corrected MORB compositions to 8% MgO using a linear approximation to the slope of the liquid line of descent. *Geist* [1992] used a similar procedure, basing his correction on a theoretical evolution model for Galápagos magmas. We have adopted this approach and corrected SiO_2, FeO, Na_2O, and K_2O abundances using Geist's equations for the Galápagos (after first recalculating analyses to 100%). $Si_{8.0}$, $Fe_{8.0}$, $Na_{8.0}$, and $K_{8.0}$ for representative samples are reported in Table 1. For incompatible elements, however, the linear correction functions of *Klein and Langmuir* [1987] and *Geist* [1992] are not satisfactory from both theoretical and observational perspectives. Theoretically, fractional crystallization produces an exponential increase in incompatible element abundances as a function of the fraction of liquid remaining. An exponential increase is precisely what we observe when incompatible elements are plotted against MgO (Figure 13). Thus to facilitate comparison of incompatible element abundances and minimize the effects of fractional crystallization, we also applied corrections to La, Sm, and Yb abundances using equations of the form $M_{8.0} = M \times e^{a(MgO-8.0)}$, where M is the concentration of the element of interest and the coefficient a was derived empirically from the relationship between these elements and MgO for the entire Galápagos data set.

Obviously, caution must be used in applying such corrections so as not to impose artificial relationships between variables, and not to obscure real ones. Our attempt at correcting the data had mixed results. For SiO_2, Na_2O, K_2O, La, Sm, and Yb, applying the corrections reduced the scatter of the data for individual volcanos as well as reducing correlations with MgO and Mg#, suggesting the correction procedure at least reduced the effects of fractional crystallization on the abundances of these elements. The abundances of these elements bear comparatively simple relationships to MgO concentration (Figures 2, 3, and 13). Ba, however, was not significantly correlated with MgO, so we did not apply a correction; apparently, the effects of fractional crystallization on Ba are small compared to degree of melting and source effects. In the case of ΣFeO, a significant, though reduced, correlation remained even after correction. This may reflect the correlation between MgO and FeO in primary melts [e.g., *Hanson and Langmuir*, 1978], or it could reflect the complexity of the relationship between FeO and MgO in the raw data (Figure 2) and the inadequacy of the correction we applied. *Geist* [1992] also reported correction terms for the CaO/Al_2O_3 ratio, but we found that applying this correction resulted in a stronger correlation with MgO than existed in the raw data. The complex relationship between CaO/Al_2O_3 and MgO (Figure 2) suggests no simple correction can be applied to this parameter, so we did not consider it further. By computing corrected La, Sm, and Yb abundances, we were also able to calculate corrected La/Sm and Sm/Yb ratios. The corrected La/Sm ratios correlated slightly better with isotope ratios than did the uncorrected ratios. This suggests our correction was essentially sound, since La/Sm depends strongly on source composition. In the discussion that follows we use the notation of *Klein and Langmuir* [1987] to denote corrected variables.

To examine the relationship between the various chemical and isotopic parameters, we calculated average values for each volcano (Table 6), and then computed the correlation matrix (Table 7) for these averages. La/Sm ratios and Ba and La

TABLE 3. Isotope Ratios in Galapagos Lavas

Sample	Location	$^{87}Sr/^{86}Sr$	$^{143}Nd/^{144}Nd$	$^{206}Pb/^{204}Pb$	$^{207}Pb/^{204}Pb$	$^{208}Pb/^{204}Pb$
Española						
E-102	Summit	0.70294	0.513024			
G86-2*	Gardner Bay	0.70298	0.513027	18.725	15.520	38.289
G86-3*	Punta Suarez	0.70292	0.513044	18.762	15.535	38.380
H334	Punta Suarez	0.70293	0.513021	18.742	15.522	38.309
Fernandina						
E-42		0.70312	0.51294	19.064	15.553	38.696
F436†	1961 Flow	0.70319				
F3N3†		0.70323				
E-87	P. Espinoza	0.70320	0.512934			
E-41	So. slope	0.70319	0.512951	19.114	15.567	38.778
Floreana						
E-98	wehrilite xenolith	0.70352	0.512937	19.970	15.664	39.721
FL-3	Main Series	0.70366	0.512905	20.002	15.657	39.739
FL-19*	Main Series	0.70340	0.512928	19.812	15.642	39.469
FL-25*	Flank Series	0.70339	0.512968	19.606	15.622	39.254
FL-26	Flank Series	0.70343	0.512929			
FL-27	Flank Series	0.70338	0.512971			
FL-29*	Main Series	0.70353	0.512936	20.004	15.666	39.746
E-110	Flank Series	0.70360	0.512975	19.785	15.636	39.516
E-108	Flank Series	0.70341	0.512954	19.605	15.605	39.283
Genovesa						
E-169		0.70272	0.513127	18.387	15.511	37.941
E-171		0.70266	0.513119	18.433	15.517	37.976
E-172		0.70259	0.513119	18.443	15.524	38.005
G303		0.70274	0.513142			
G86-8*		0.70275	0.513116	18.439	15.511	37.967
G304	P.rince Philip's Steps	0.70270	0.513107	18.427	15.509	37.952
Isabela						
E-132*	Volcan Alcedo	0.70331	0.512939	19.337	15.576	38.955
E-134	Volcan Alcedo	0.70327	0.512996			
E-135*	Volcan Alcedo	0.70316	0.512988	19.119	15.559	38.673
E-137	Volcan Alcedo	0.70309	0.512978	19.191	15.58	38.806
B056†	Volcan Ecuador	0.70297				
B155†	Volcan Ecuador	0.70297	0.513006			
E-54	Volcan Ecuador	0.70328	0.512940	19.232	15.597	38.951
E-56	Volcan Ecuador	0.70322	0.512932	19.274	15.593	38.990
Z0B6†	Cerro Azul	0.70332	0.512931			
CA90-1*	Cerro Azul	0.70336	0.512933	19.317	15.568	38.955
CA90-6*	Cerro Azul	0.70334	0.512954	19.322	15.573	38.947
N0C5†	Sierra Negra	0.70338	0.512922			
SN-1	Sierra Negra	0.70330	0.512915	19.372	15.602	39.058
SN-3	Sierra Negra	0.70332	0.512931	19.375	15.604	39.073
E-152	Volcan Wolf	0.70275	0.513047	18.971	15.588	38.474
E-153	Volcan Wolf	0.70269	0.513077	18.822	15.554	38.426
E-155	Volcan Wolf	0.70273	0.513038	18.908	15.542	38.38
E-151*	Volcan Darwin	0.70285	0.513005	18.788	15.525	38.277
E-216*	Volcan Darwin	0.70289	0.512982	18.813	15.542	38.364
E-217*	Volcan Darwin	0.70282	0.513022	18.79	15.545	38.331
E-224*	Volcan Darwin	0.70286	0.513005	18.801	15.545	38.43
E-237*	Volcan Darwin	0.70276	0.513053	18.686	15.519	38.167
E-242*	Volcan Darwin	0.70289	0.512994	18.765	15.514	38.231
E-243*	Volcan Darwin	0.70285	0.513005	18.794	15.544	38.341
E-63	Volcan Darwin (Tagus C)	0.70278	0.513016	18.787	15.533	38.318
Marchena						
E-15		0.70276	0.513048			
M-28		0.70280	0.513035			
M-34		0.70280	0.513047			
M-39		0.70287	0.513046			
M-51		0.70281	0.513027			
M-63		0.70277	0.513036	18.923	15.557	38.521
M-67		0.70278	0.513039			
M071†		0.70281	0.513043			
M10		0.70287	0.513021	18.91	15.558	38.522
M12		0.70291	0.513036			
M31groundmass	0.70276	0.513037				
M31plagioclase	0.70277	0.513033				
M069†	Caldera Wall	0.70285				
Pinta Island						
E-4		0.70329	0.512902			
E-8		0.70331	0.512887	19.346	15.631	39.302
P-24 plagioclase	0.70314	0.512922				
P-24 groundmass	0.70313	0.512943				
P-42		0.70338	0.512892	19.228	15.63	39.208

TABLE 3. (continued)

Sample	Location	$^{87}Sr/^{86}Sr$	$^{143}Nd/^{144}Nd$	$^{206}Pb/^{204}Pb$	$^{207}Pb/^{204}Pb$	$^{208}Pb/^{204}Pb$
P-50		0.70319	0.512923	19.139	15.604	39.024
San Cristobal						
E-103	Southwest	0.70281	0.513042	18.838	15.536	38.386
SC-9*	Southwest	0.70287	0.513074	18.888	15.543	38.491
SC-20*	Southwest	0.70315	0.513023	18.974	15.548	38.558
SC-28*	Southwest	0.70284	0.513074	18.800	15.516	38.334
SC-34*	Southwest	0.70312	0.513032	18.794	15.550	38.433
SC-123	Northeast	0.70327	0.513047	18.776	15.558	38.430
SC-59	Northeast	0.70310	0.513030	18.729	15.549	38.369
SC-61	Northeast	0.70293	0.513006	18.824	15.562	38.484
SC-75	Northeast	0.70293	0.513052	18.702	15.552	38.378
C-332	Northeast	0.70312	0.513063			
Pinzon						
E-68b		0.70298	0.512988			
E-70		0.70311	0.513018	19.005	15.557	38.569
PS-16*		0.70291	0.512997	19.031	15.568	38.610
Rabida Island						
E-51*		0.70300	0.512980	19.028	15.553	38.611
E-174		0.70297	0.513013			
G86-10*		0.70300	0.513013	19.142	15.568	38.746
Santa Cruz						
E-1	Academy Bay (Shield)	0.70263	0.513077	18.514	15.52	38.048
SC-46	Academy Bay (Shield)	0.70262	0.513088			
SC-64	NW (Shield)	0.70274	0.513059			
SC-78	N. Coast (Shield)	0.70262	0.513101			
SC-100	NE Shield	0.70266	0.513074	18.656	15.521	38.147
SC-151	South Shield	0.70268	0.513094			
SC-161	Summit (Shield)	0.70263	0.513085	18.511	15.517	38.032
SC-163	SE Shield	0.70267	0.513063	18.555	15.508	38.016
SC-200	Summit (Shield)	0.70261	0.513086	18.513	15.515	38.019
SC-108	NE Platform	0.70289	0.513020	18.774	15.564	38.45
SC-174	North Central, Platform	0.70286	0.513043	18.714	15.543	38.288
SC-196	NE Platform	0.70283	0.513014			
SC-83	NE Platform	0.70281	0.513040	18.774	15.564	38.45
G86-1*	South Las Plazas (Platform)	0.70296	0.513022	18.686	15.531	38.266
E-167	Seymour Island (Platform)	0.70312	0.512997	18.946	15.566	38.553
E-31	Baltra Island (Platform)	0.70306	0.513034	18.719	15.556	38.337
Santa Fe Island						
E-111		0.70300	0.513033			
G86-4*		0.70318	0.512980	18.814	15.548	38.504
G86-5*		0.70330	0.512934	18.965	15.584	38.807
SF-13		0.70293	0.513005	18.722	15.569	38.475
Santiago Island						
SH-7*	NW Highlands	0.70281	0.513053	18.843	15.559	38.446
SH-75a	1897 Flow (NW)	0.70275	0.513045	18.599	15.534	38.197
E-16	James Bay (NW)	0.70279	0.513027	18.856	15.549	38.404
E-20	Marmalade Pot Flow(NW)	0.70294	0.512980	19.022	15.582	38.726
E-76	Buccaneer Cove (NW)	0.70286	0.513002	19.05	15.58	38.656
E-24	Sullivan Bay (SE)	0.70272	0.513029			
JL-94*	SE flank	0.70277	0.513045	18.701	15.543	38.285
JH-86*	Eastern Highlands	0.70280	0.513057	18.554	15.550	38.164
BL-1*	Bartolomé, S.E.	0.70279	0.513062	18.628	15.539	38.180
Wolf & Darwin Islands						
DA-1	Darwin	0.703008	0.512949	19.01	15.607	39.032
DA-2	Darwin	0.703032	0.512954	19.044	15.596	38.983
E-35	Darwin	0.70302	0.512984			
E-39	Wolf	0.70300	0.513002	19.085	15.609	38.911
WO-1	Wolf	0.70337	0.512950	19.074	15.597	38.874
Smaller Rocks and Cones						
E87-2*	Cowley Island	0.70306	0.512981	19.184	15.583	38.803
E87-1*	Nameless Rock	0.70714	0.513051	18.716	15.545	38.281
E-156	Roca Redonda	0.70311	0.512964	19.334	15.599	39.048

Except where noted, values were determined at the Max-Plank-Institut in Mainz (MPI). $^{87}Sr/^{86}Sr$ is corrected for mass fractionation by normalizing to $^{86}Sr/^{88}Sr = 0.11940$. Values are reported relative to $^{87}Sr/^{86}Sr = 0.70800$ for the Eimer and Amend (E&A) Sr isotope standard. Actual measured values were 0.70792 at DTM, 0.70800 at MPI, and 0.70802 at Cornell. Estimated analytical uncertainties are ±0.00006 for the DTM data and ±0.000035 for the MPI and Cornell data (2σ). $^{143}Nd/^{144}Nd$ is corrected for mass fractionation by normalizing to $^{146}Nd/^{144}Nd = 0.72190$. Values are reported relative to $^{143}Nd/^{144}Nd = 0.51264$ for U.S. Geological Survey standard BCR-1. Actual measured values for BCR-1 were 0.512695 at DTM, 0.512647 at MPI, and 0.512643 at Cornell. Measured values for the La Jolla Nd isotopic standard were 0.511847 at MPI and 0.511840 at Cornell. Estimated analytical uncertainties are ±0.000040 for the DTM data, ±0.000020 for the MPI, and ±0.000016 for the Cornell data (2σ). Pb isotope ratios are reported relative to values of $^{206}Pb/^{204}Pb = 16.937$, $^{207}Pb/^{204}Pb = 15.493$, and $^{08}Pb/^{204}Pb = 36.705$ for the NBS-981 standard. A fractionation correction of 1.40‰ per amu and 1.10‰ per amu has been applied to the MPI and Cornell data, respectively. Estimated analytical uncertainties are $^{206}Pb/^{204}Pb$ ±0.010, $^{207}Pb/^{204}Pb$: ±0.016, and $^{208}Pb/^{204}Pb$: ±0.035 (2σ)

† Determined at the Department of Terrestrial Magnetism (DTM).

* Determined at Cornell University (Cornell).

TABLE 4. Comparison of $^{87}Sr/^{86}Sr$ in Leached and Unleached Galapagos Basalts

	Unleached	Leached
E-4	0.70387	0.70329
SC-59	0.70329	0.70310
SC-196	0.70399	0.70293
E-111	0.70341	0.70300
WO-1	0.70345	0.70337
FL-3	0.70395	0.70366

concentrations strongly correlate with isotope ratios. With the exception of $K_{8.0}$, none of the major element abundances are correlated with isotope ratios or with La/Sm. $Na_{8.0}$ correlates with $K_{8.0}$ and weakly with $Sm_{8.0}$ and $Yb_{8.0}$. $Si_{8.0}$ shows a weak inverse correlation with $Sm/Yb_{8.0}$. Fe correlates with no other parameter. Within individual volcanic suites $Na_{8.0}$ does seem to correlate strongly with $La/Sm_{8.0}$ in some cases (Figure 14). The Santa Cruz shield series, San Cristobal, Cerro Azul, Santiago, and Santa Fe all appear to exhibit such a correlation. This correlation probably results from the melting process, which affects both Na_2O concentrations and La/Sm ratios. In most other cases, there are too few data to establish whether a correlation exists. No within-suite correlations were observed between major elements and isotope ratios.

Geographic Patterns

Perhaps the most remarkable feature of the Galápagos is the systematic variation in isotope ratios, in which the most depleted isotopic signatures occur in the center of the archipelago and the most enriched signatures occur on the southern, western, and eastern margins. This pattern was first noted by *White and Hofmann* [1978] for Sr isotope ratios. The present results entirely confirm the earlier findings. Further, this zonation can be observed in Pb and Nd isotope ratios and incompatible element ratios as well. The patterns for $^{87}Sr/^{86}Sr$, ε_{Nd}, La/Sm_N, and Sm/Yb_N are shown as computer-generated contour plots in Figure 15. Contours are based on averages for individual volcanos, with locations backtracked to the point where the lava was erupted (i.e., corrected for plate motion). Separate averages were made for islands showing a range of ages or a geographic compositional variations (Floreana, San Cristobal, Santiago, Santa Cruz). Data for basalts dredged from the Galápagos Spreading Center [*Schilling et al.*, 1982; *Verma and Schilling*, 1982; *Verma et al.*, 1983] were also used in the contouring. Contours were closed on the assumption that normal (i.e, average MORB) oceanic crust surrounds the Galápagos Platform.

The geographic patterns of $^{87}Sr/^{86}Sr$, ε_{Nd}, and La/Sm_N are similar: they are horseshoe-shaped with the most depleted signatures in the northeastern and central parts of the archipelago. They differ in detail: maximum $^{87}Sr/^{86}Sr$ and La/Sm_N occur on Floreana in the south, while two minima for ε_{Nd} occur; one on Pinta in the north, and the other on Floreana in the south, though a secondary maximum for $^{87}Sr/^{86}Sr$ occurs on Pinta. The pattern for Pb isotope ratios (not shown) is essentially similar to that of $^{87}Sr/^{86}Sr$, with the maximum on Floreana. Contours of other incompatible element ratios (e.g., Rb/Sr) and incompatible element concentrations generally show the same horseshoe shape. The pattern for $Sm/Yb_{N8.0}$ differs somewhat from those of the other ratios shown; rather than a horseshoe, $Sm/Yb_{N8.0}$ is highest in the western part of the archipelago, with maxima at Cerro Azul and Volcan Ecuador, the northern and southernmost volcanos on Isabela.

The contours for isotope and incompatible element ratios are nearly parallel to the lithospheric fault system that M. A. Feighner and M. A. Richards (submitted manuscript, 1993) infer divides strong lithosphere to the south and west from weak lithosphere to the north and east, with the more depleted compositions occurring in the region of weak lithosphere. There are important differences, however. Wolf and Darwin volcanos have fairly depleted isotopic signatures yet lie upon strong lithosphere while Pinta, which has a strongly enriched isotopic signature, apparently lies on weak lithosphere.

Figure 15 illustrates another intriguing feature of Galápagos geochemistry: the most enriched isotopic signatures on the GSC do not occur at its closest approach to the Galápagos, rather they lie northwest of the archipelago, at the intersection of the Wolf-Darwin lineament with the GSC. If there is flow of plume

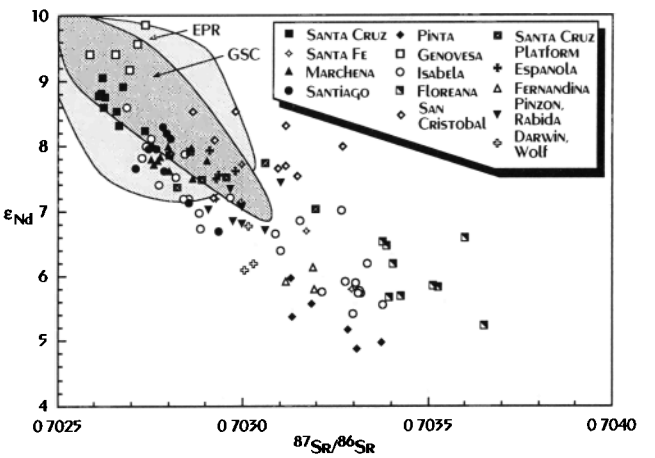

Fig. 6. ε_{Nd} and $^{87}Sr/^{86}Sr$ ratios of Galápagos lavas. Light shaded region shows the field for East Pacific Rise MORB; dark shaded region is the field for GSC MORB.

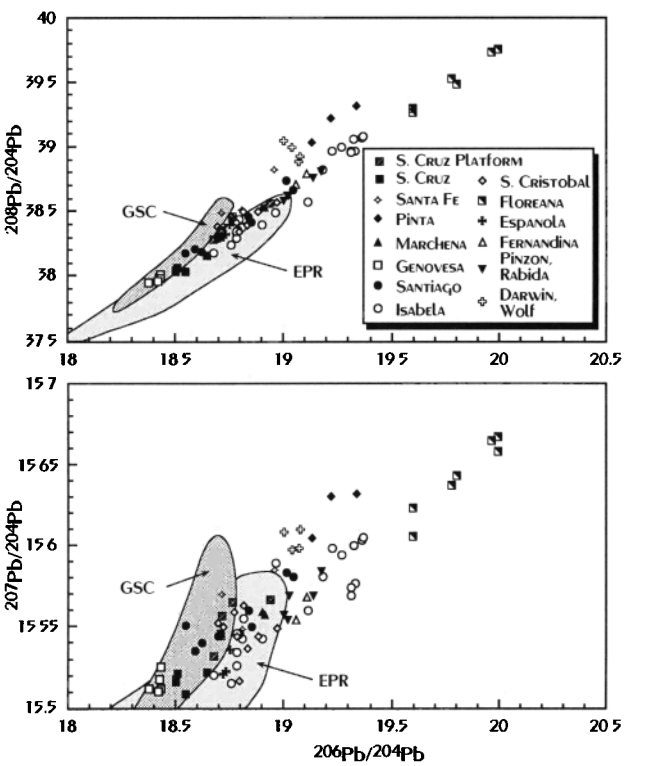

Fig. 7. Pb isotope ratios of Galápagos lavas. Light shaded region shows the field for East Pacific Rise MORB; dark shaded region is the field for GSC MORB.

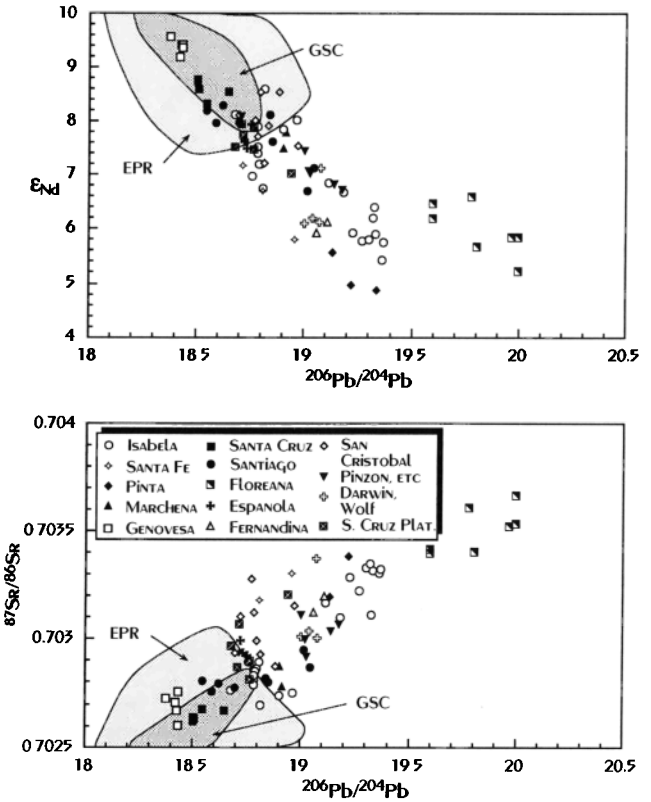

Fig. 8. ε_{Nd} and $^{87}Sr/^{86}Sr$ for Galápagos lavas plotted against $^{206}Pb/^{204}Pb$. Light shaded region shows the field for East Pacific Rise MORB; dark shaded region is the field for GSC MORB.

material from the Galápagos to the GSC, as Schilling and coworkers have suggested [*Schilling et al.*, 1982; *Verma and Schilling*, 1982; *Verma et al.*, 1983], then flow is "upstream" in the sense that regional plate motion, and presumably uppermost asthenosphere motion, is to the east-southeast (100.5°).

Geographic patterns for the major elements are not as well developed as those of isotope and incompatible element ratios, but some general features are apparent: $Na_{8.0}$ is lowest in the west central volcanos but also decreases toward the GSC; $Si_{8.0}$ appears to show a broad, weak minimum over the west central part of the archipelago and may also increase toward the GSC; $Fe_{8.0}$ is lowest in the northwestern volcanos and highest in the volcanos of the central part of the archipelago, with a maximum on Santiago. These patterns are similar to those found by *Geist* [1992] using a different, but overlapping, data set. *Geist* [1992] concluded that magmas from the center of the archipelago are derived by a relatively low average extent of melting and deeper average extraction depths.

Discussion

The distribution and composition of volcanic activity in the Galápagos region present a number of puzzling features that require explanation. These include the following: the number of simultaneously active volcanos in the Galápagos archipelago; the east-west differences in size and structure of volcanos; the extended period of volcanism on a number of islands, most notably San Cristobal, Santa Cruz, and Santa Fe; the restriction of differentiated rocks to the center of the archipelago; the lower SiO_2 content of Galápagos lavas relative to MORB; the great variety of isotope and trace element compositions displayed by Galápagos lavas; the presence of lavas with isotope ratio and incompatible element characteristics indistinguishable from MORB; the geographic zonation of isotope ratios and incompatible element concentrations and ratios, with the most depleted signatures occurring in the central and northeast part of the archipelago; and the north-south differences in geochemistry: e.g., lavas from the southern islands, particularly Floreana, have higher La/Sm_N, $^{206}Pb/^{204}Pb$ and $^{87}Sr/^{86}Sr$ at the same ε_{Nd} compared with northern islands.

Geographic Patterns of Isotope Ratios and Plume-Asthenosphere Dynamics

The geographic elemental and isotopic variations raise the most fundamental questions, and we discuss them first. We considered four types of models to explain the observed chemical variations. The first model is that of a plume heterogeneous on a scale of 10-100 m, with incompatible element-enriched veins or lenses that melt at lower temperature than the more depleted matrix in which they are embedded, i.e., the veined, or plum-pudding mantle considered by *Hanson* [1977], *Morris and Hart* [1983], *Batiza and Vanko* [1984], and *Zindler et al.* [1984]. The plume is hottest in its center, so melting there would proceed to a higher degree, and melts produced would reflect a higher contribution from the depleted, higher solidus matrix. In the second model, a chemically homogenous plume impinges on the overlying lithosphere and heats and melts it. The western volcanos would reflect melting of the plume, while those to the east and over the central axis of the hotspot track would reflect an increased contribution from remelting of the depleted lithosphere (M. A. Feighner and M. A. Richards, submitted manuscript, 1993). In the third model, isotopic and incompatible element variations reflect entrainment of asthenosphere into the center the plume. In the fourth model, relict asthenospheric upwelling, reflecting the former position of the GSC, produces extensional tectonism and persistent volcanism of more MORB-like composition along the central axis and northern margin of the platform.

The first of these models predicts a relationship between degree of melting and isotope ratios, while the second predicts a relationship between magma chemistry, particularly isotope ratios, and depth of melting. Degree of melting has a strong influence on magma chemistry, independent of source composition, which affords an opportunity to test these models. These influences of depth and degree of melting on magma chemistry have been reviewed by *Klein and Langmuir* [1987, 1989], and *Geist* [1992] has discussed them in the context of Galápagos geochemistry. As *Klein and Langmuir* [1987, 1989] have pointed out, Na is a moderately incompatible element, and its concentration should be inversely related to degree of melting. Experimental observations show that the Na_2O concentration of partial melts is essentially independent of pressure and that SiO_2 and FeO are sensitive to both degree and depth of melting [e.g., *Jaques and Green*, 1980]. SiO_2 increases with increasing degree of melting and decreases with increasing depth, while FeO increases with depth and decreases as degree of melting increases in an upwelling column.

If the isotopic variations in the Galápagos reflect varying degrees of melting of a plum-pudding mantle, $^{87}Sr/^{86}Sr$, for example, should show a positive correlation with Na_2O, and an inverse one with SiO_2 if depth of melting were constant. Table 7 shows clearly that this is not the case. Indeed, average $Na_{8.0}$ is highest on Santa Cruz, where isotope ratios approach those of MORB, and lowest on the central and southwestern volcanos and Fernandina in particular. If the $Na_{8.0}$ value can be taken as an indicator of relative degree of melting as suggested by *Klein and*

TABLE 5. Trace Element Concentrations in Galápagos Lavas

	La	Ce	Pr	Nd	Sm	Eu	Gd	Tb	Dy	Ho	Er	Tm	Yb	Lu	K_2O	Rb	Cs	Sr	Ba	Y	Zr*	Cr*	Co*	Ni*
Santa Cruz																								
SC-174	11.10	28.5		18.70	5.02	1.69	5.96		6.42		3.87		3.60	0.543	0.620	6.90	0.033	223	53.9			159	32	43
SC-78	2.97	9.02		7.54	2.31	0.93	2.99		3.41		2.09		1.87	0.290	0.083	1.04	0.013	212	12.7		76			325
SC-64	2.98	9.00		7.51	2.31	0.95	3.00		3.41		2.09		1.95	0.296	0.094	0.61	0.010	236	13.6		78	442	33	244
E-1	9.79	28.2		20.10	5.17	1.85	5.71		5.64		3.20		2.85	0.423	0.259	3.15	0.041	409	42.5		188	340	67	400
SC-163	13.10	33.7		23.50	5.83	2.02	6.57		6.57		3.87		3.54	0.542	0.267	1.39	0.072	370	56.5		218	168	32	135
SC-100	2.58	7.54		6.24	1.97	0.82	2.77		3.45		2.24		2.16		0.090	0.84	0.006	226	17.6		62			155
SC-196	10.70	27.6		19.40	5.42	1.94	6.49		6.75		3.83		3.41	0.512	0.348	4.71	0.049	252	62.5		180			73
SC-151	25.20	65.3		39.30	9.01	2.99	9.12		8.76		4.97		4.56	0.693	0.191	9.95	0.130	457	121.0		423	92	25	55
SC-83	11.60	31.9		22.60	6.03	2.27	6.35		7.04		4.04		3.57	0.547	0.208	1.81	0.013	319	37.8		135			46
SC-46	3.96	10.5		7.51	2.09	0.78	2.49		2.65		1.55		1.39	0.211	0.229	2.42	0.021	341			134			349
SC-161	6.80	19.5		14.30	3.79	1.40	4.23		4.47		2.62		2.39	0.360	0.195	2.28	0.035	342	29.3					
SC-108	21.00	53.8		35.80	9.66	3.20	10.70		11.60		6.61		5.90	0.864	0.678	8.76	0.100	267	119.0		312			32
SC-200	13.20	35.2		23.10	5.63	1.92	5.85		6.01		3.56		3.27	0.502	0.405	5.12	0.056	365	54.0		263			244
G86-1†	9.57	24.9	3.62	16.50	4.65	1.54	5.24	0.95	5.61	1.18	3.20	0.51	3.04	0.472					54.3					
Seymour																								
E-167	10.60	26.9		18.00	4.77	1.75	5.35		4.95		2.55		2.12	0.314	0.272	3.11	0.040	452	158.0			173	53	105
Santa Fe																								
E-111‡	2.92	8.52	1.46	7.81	2.52	1.04	3.47	0.65	3.88	0.83	2.26	0.34	2.11	0.335	0.096	0.48	0.006	211	299.0					
SF-13†	14.71	35.9	5.04	23.00	5.63	1.88	6.27	1.11	6.41	1.28	3.49	0.56	3.16	0.476	0.550	8.6		359	109.0	31.6		379	73	241
G86-5†	29.21	67.1	8.95	39.01	9.63	2.86	9.91	1.73	9.25	1.82	4.67	0.69	4.07	0.623		13.80		338	177.1	50.9				
Marchena																								
M071‡	4.41	12.5	1.88	9.33	2.78	1.12	3.58	0.65	3.61	0.77	2.08	0.31	1.86	0.273	0.153	1.78	0.017	262	26.4					
M069															0.240	2.19	0.019	210	46.0					
E-15	8.50	22.9		17.30	5.17	1.86	6.35		6.50		3.56		3.14	0.449	0.284	4.23		223	45.7					51
E-10‡	6.13	16.6	2.58	13.49	4.25	1.55	5.34	1.00	5.97	1.29	3.59	0.52	3.24	0.487	0.214	0.84	0.007	215	46.2					51
Pinta																								
E-4‡	20.86	47.9	6.56	28.50	6.91	2.17	6.58	1.15	6.70	1.29	3.43	0.49	2.95	0.428	0.718	12.8	0.109	355	172.0		200	117	53	54
E-8‡	23.22	50.9	6.62	28.00	6.43	2.15	6.73	1.08	5.75	1.12	3.01	0.43	2.78	0.416	0.755	13.4	0.096	365	177.0					44
P-50	15.50	35.6		22.30	5.77	2.02	6.51		6.47		3.56		3.12			6.6	0.018	276	122.7					
Genovesa																								
E-169	2.04	7.25		7.59	2.73	1.08	3.85		4.53		2.82		2.64	0.398	0.051	0.325	0.002	135	7.2			194	61	87
E-171†	2.58	8.85	1.67	9.50	3.34	1.252	4.57	0.88	5.38	1.17	3.17	0.49	3.04	0.469	0.12*	0.487		145	9.1	32.8		119	52	50
E-172†	2.89	9.43	1.79	10.26	3.57	1.29	5.13	0.95	5.84	1.29	3.50	0.54	3.39	0.532	0.09*			148	9.8	39.9		103	56	65
G86-8†	3.05	11.2	2.04	10.97	4.09	1.48	5.64	1.08	6.82	1.48	4.10	0.65	4.04	0.675	0.09*			135*	10.2			121	59	48
G304		8.48		8.42	3.00	1.28	4.40		4.87		3.07		2.84		0.068	0.631	0.008	141	9.3					
G303	1.95	6.97		7.45	2.68	1.08	3.76		4.48		2.78		2.61	0.387	0.056	0.243	0.006	132	6.3					
Isabela																								
B155		53.4		31.40	7.61	2.61	8.35		7.40		3.61		2.97		0.701	10.5	0.050	409	147.0					
E-56	21.00	48.4		28.70	6.96	2.37	7.18		6.37		3.25		2.70	0.398	0.784	11.8	.059	374	171.2			207	54	85
B056															0.858	12.2	0.127	429	174.0					
E-63	16.10	41.1		26.70	6.77	2.26	7.28		6.69		3.50		2.93	0.434	0.518	6.07	0.068	347	64.0		255	142	55	70
E-132‡	10.46	24.0	3.23	14.93	3.94	1.39	4.86	0.81	4.78	1.01	2.72	0.41	2.47	0.375	0.373	6.78	0.092	280	95.9	27.9				53

TABLE 5. (continued)

	La	Ce	Pr	Nd	Sm	Eu	Gd	Tb	Dy	Ho	Er	Tm	Yb	Lu	K_2O	Rb	Cs	Sr	Ba	Y	Zr*	Cr*	Co*	Ni*
E-134		22.9		15.10	4.08	1.59	4.50		4.52		2.44		2.08		0.292	4.56	0.055	294	50.2					65
E-135†	66.52	136.3	17.7	71.43	16.79	2.93	15.21	2.72	16.5	3.66	10.4	1.62	10.1	1.56	3.11*	66.0		81	381.4	91.1		6.8	12	7.5
E-137†	14.87	36.3	5.14	23.58	6.15	2.005	6.91	1.19	6.58	1.29	3.29	0.49	2.89	0.433	0.25*	5.39		286	77.1	37.0		109	56	62
E-152†	14.14	36.8	5.27	22.97	5.98	2.05	6.39	1.13	5.87	1.16	2.91	0.42	2.48	0.368	0.41*	6.0*		424*	52.7			207	54	85
E-153†	18.99	49.1	7.06	31.19	8.15	2.61	8.15	1.43	7.72	1.48	3.88	0.56	3.32	0.487	0.770	3.0*		387*	75.5			51	54	50
E-155†	12.81	32.8	4.82	22.57	5.88	1.962	6.46	1.10	5.92	1.14	2.85	0.43	2.42	0.360	0.36*	4.0*		389*	53.2			159	43	65
E-156	18.10	41.4		24.00	5.93	2.01	6.13		5.50		2.84		2.39	0.346	0.643	11.5	0.126	346	153.0			692	82	459
E-216†	19.53	49.1	6.99	31.88	7.91	2.52	8.43	1.47	7.92	1.55	3.98	0.57	3.53	0.532	0.61*	7.73		344	84.4	39.1		65	47	50
E-217†	9.62	24.8	3.58	16.59	4.29	1.48	4.60	0.81	4.37	0.86	2.21	0.32	1.93	0.289	0.37*	3.67		379	41.3	21.9		276	43	86
E-224†	26.76	66.5	9.37	41.92	10.32	3.04	10.92	1.84	9.84	1.94	4.92	0.73	4.38	0.654	0.88*	13.7		329	102.0	50.6		24	43	33
E-237†	21.38	55.1	7.97	35.90	9.01	2.803	9.69	1.61	8.65	1.71	4.32	0.64	3.81	0.576	0.69*	8.53	0.000	373	77.9	44.4		22	47	28
E-242†	14.23	36.2	5.19	23.55	5.99	2.02	6.62	1.10	5.81	1.13	2.82	0.42	2.44	0.367	0.47*	5.05		362	55.8	29.5		65	42	59
E-243†	15.52	39.4	5.72	26.14	6.77	2.26	7.63	1.28	6.92	1.36	3.44	0.50	3.04	0.449	0.52*	10.0*		285*	63.4			37	42	45
N0C5		40.7		25.10	6.33	2.31	7.02		6.28		3.45		2.97		0.504	9.00	0.099	289	108.0					
SN-1†	19.55	45.3	6.34	27.92	7.03	2.24	7.34	1.28	6.93	1.35	3.57	0.51	3.11	0.455	0.57*	13.4		295	125.7	34.4		93	47	52
SN-3†	24.50	57.2	7.76	33.57	8.50	2.62	8.75	1.51	8.23	1.63	4.21	0.61	3.76	0.560	0.58*	16.6		394	153.1	51.9				
Z0B6‡	17.86	40.1	5.25	22.30	5.17	1.85	5.40	0.86	4.63	0.92	2.45	0.37	2.12	0.312	0.875	16.1	0.174	386	210.0					
Fernandina																								
F3N3															0.270	4.10	0.028	213	59.8					
F436															0.443	7.44	0.082	356	96.1					
E-87‡	13.78	33.8	4.69	21.00	5.40	2.01	5.95	1.02	5.43	1.09	2.89	0.41	2.40	0.351	0.372	6.53	0.116	328	83.6					
E-42	13.80	33.5		21.30	5.43	1.90	5.96		5.66		2.91		2.50	0.351	0.423	7.07	0.081	329	89.8		182	479	48	68
Santiago																								
E-20	11.40	28.2		19.10	5.22	1.80	6.07		5.84		3.13		2.70	0.407	0.369	5.96	0.057	473	60.4					204
E-24	5.01	14.1		10.60	3.03	1.14	3.82		4.28		2.62		2.46	0.365	0.143	1.39	0.010	243	25.3					232
E-76‡	7.17	17.9	2.59	12.00	3.33	1.21	3.97	0.70	3.98	0.79	2.07	0.30	1.80	0.273	0.226	2.29	0.018	284	38.8					153
SH-75a		8.91		7.45	2.39	1.03	3.32		3.67		2.33		2.20		0.077	0.86	0.010	193	11.9					
SH-7†	8.19	21.9	3.31	16.44	4.55	1.65	5.71	0.99	5.84	1.21	3.28	0.49	3.09	0.477	0.31*	7.0*		276*	42.3		155	187	52	104
JL-94†	4.69	12.7	2.05	10.07	3.00	1.10	3.89	0.72	4.19	0.89	2.41	0.36	2.30	0.359	0.10*			271*	24.0		96	380	53	246
JH-86†	3.06	9.19	1.55	8.17	2.50	0.97	3.27	0.59	3.58	0.75	2.05	0.32	1.97	0.296	0.05*	1.55		221	16.3	19.7				
BL-1†	3.51	10.2	1.67	8.60	2.58	1.01	3.49	0.63	3.87	0.82	2.30	0.35	2.19	0.342	0.10*	5.0*		198*	16.2			256	54	162
Floreana																								
E-110	16.80	31.7		15.70	3.63	1.2	4.05		4.15		2.42		2.22	0.356	0.900	21.4	0.229	265	16.8		122	1250	76	428
FL-3	14.90	26.3		11.40	2.49	0.88	2.87		3.07		1.90		1.79	0.283	1.077	20.0	0.152	505	620.0		61			372
FL-19†	41.64	68.2	6.92	23.25	3.85	1.23	3.72	0.68	3.73	0.78	2.17	0.33	2.27	0.367	1.30*	38.6		504	667.1	22.9	142	297	66	126
FL-25†	9.71	18.6	2.44	10.57	2.74	0.99	3.36	0.63	3.66	0.75	2.07	0.30	1.97	0.302	0.26*	6.75		323	137.6		60	427	50	212
FL-26‡	8.56	17.5	2.28	9.81	2.51	0.89	2.90	0.51	3.12	0.67	1.90	0.30	1.83	0.291	0.264	4.14	0.030	271	110.0		57	369	52	188
FL-27	13.20	25.1		12.90	3.23	1.19	3.83		4.09		2.43		2.25	0.350	0.850	19.5		353	260.0		92			84
FL-29†	12.38	21.6	2.57	10.26	2.41	0.83	2.84	0.53	2.96	0.63	1.75	0.27	1.68	0.266	0.93*	17.9		435	324.6		62	726	52	354
E-98	2.84	6.70		4.63	1.48	0.57	2.24		2.73		1.65		1.45	0.214	0.023	0.59	0.012	52.3	11.8					
Espanola																								
E-102‡	12.24	27.2	3.61	15.80	3.86	1.45	4.32	0.81	4.60	0.99	2.73	0.42	2.53	0.375	0.364	6.78	0.205	315	88.3					240
H334		33.1		18.30	4.41	1.67	5.06		5.63				3.27		0.460	6.03	0.042	374	65.2					
G86-3†	15.73	34.9	4.57	19.66	4.62	1.52	5.18	0.93	5.36	1.11	2.99	0.45	2.78	0.425		10.1		384	108.9	31.0		330	59	197

TABLE 5. (continued)

	La	Ce	Pr	Nd	Sm	Eu	Gd	Tb	Dy	Ho	Er	Tm	Yb	Lu	K_2O	Rb	Cs	Sr	Ba	Y	Zr*	Cr*	Co*	Ni*
San Cristobal																								
C-332‡	4.59	11.5	1.72	8.17	2.54	0.95	3.35	0.64	3.87	0.86	2.52	0.40	2.47	0.378	0.199	1.44	0.011	221	32.0					
E-103‡	17.41	36.0	4.80	20.50	4.91	1.64	5.55	0.98	5.63	1.22	3.49	0.52	3.09	0.489	0.765	11.4		397	221.0					
SC-9†	13.79	30.7	4.05	17.90	4.31	1.46	4.80	0.85	4.81	1.02	2.73	0.41	2.52	0.392	0.74*	10.3		407	153.8	28.4		543	66	245
SC-28†	14.23	33.5	4.58	20.28	5.08	1.66	5.72	1.02	6.00	1.25	3.43	0.53	3.25	0.511	0.58*	8.8*		378*	132.7			292	59	126
SC-59†	2.85	7.77	1.21	6.02	1.91	0.73	2.74	0.55	3.55	0.80	2.35	0.37	2.40	0.378	0.15*	1.34		164	28.8	24.5		260	61	142
SC-75†	3.97	10.6	1.66	8.41	2.63	0.97	3.45	0.69	4.22	0.96	2.64	0.42	2.62	0.403	0.18*	1.20		184	29.4	25.8		523	69	235
SC-123†	4.01	10.9	1.65	8.10	2.55	0.93	3.39	0.68	4.31	0.98	2.88	0.45	2.85	0.462	0.20*	2.0*		206*	37.9			224	59	148
Pinzon																								
PS-16†	8.98	21.9	3.22	14.91	4.11	1.39	4.86	0.85	4.65	0.96	2.42	0.35	2.11	0.321	0.27*	3.92		279	45.5	25.9	128	292	47	160
E-68b‡	20.07	44.7	6.26	29.70	7.79	2.36	9.47	1.74	9.77	1.91	5.02	0.65	3.58	0.522	0.607	7.68	0.031	296	110.0					
Rabida																								
G86-10†	25.9	59.9	8.21	36.49	8.77	2.72	9.40	1.54	8.33	1.60	4.07	0.59	3.46	0.52	0.85*	17.0*		343*	149.7			137	44	
E-51‡	35.11	88.5	12.4	54.9	13.7	4.25	14.90	2.48	13.70	2.71	6.96	1.00	5.63	0.917	0.963	13.9	0.088	334	177.0					
Darwin Island																								
DA-1†	10.26	22.7	3.18	15.04	4.37	1.45	5.51	1.02	6.06	1.31	3.59	0.55	3.41	0.525	0.37*	9.29		181	88.3	36.2		294	46	88
E-35	9.00	20.9		14.50	4.24	1.60	5.25		6.12		3.42		3.05	0.439	0.323	4.33	0.017	185	89.1			289	49	78
Wolf Island																								
WO-1†	7.14	17.2	2.45	11.51	3.19	1.17	3.91	0.73	4.15	0.86	2.35	0.36	2.25	0.344					53.4					
E-39‡	4.36	10.4	1.52	6.93	1.94	0.83	2.36	0.40	2.46	0.52	1.44	0.22	1.30	0.189	0.192	1.61	0.013	250	31.8			162	38	52
Nameless Rock																								
E87-1†	16.13	36.5	5.24	23.24	5.77	1.87	5.36	0.97	5.58	1.19	3.26	0.49	3.02	0.462	0.38*	20.5		1022	185.5	29.6		182	50	126
Cowley Island																								
E87-2†	13.59	33.8	4.68	21.96	5.86	1.94	6.33	1.10	5.92	1.15	2.90	0.42	2.52	0.368	0.46	10.6		175	79.3			127	62	124
U.S. Geological Survey Standard BHVO-1																								
TIMS§	15.74	37.7		24.81	6.10	2.03	6.44		5.36		2.43		2.02	.302	0.524	9.66	0.97	400	133.5					
± 1 σ, %	0.04	0.4		0.2	0.01	2.4	2.64		0.3		2.62		0.4	3.3	0.06	3.4	1.3	0.1	0.55					
ICP-MS¶	15.46	37.8	5.43	24.80	6.11	2.00	6.49	1.04	5.41	1.01	2.46	0.34	2.01	.293		9.53		396	132.6	24.9				
± 1 σ, %	1.8	1.6	1.5	1.1	1.1	1.8	1.3	1.6	1.5	3.2	2.6	2.8	2.7	2.9		1.9		0.8	4.1	0.9				

All Analyses by TIMS-ID except where noted. All concentrations are in parts per million, exccpt K_2O, which is in percent.

* Atomic adsorption analysis at the University of Oregon

† ICP-MS analysis

‡Combined TIMS-ID and ICP-MS analysis

§Mean and standard deviation (in percent of mean) of three thermal ionization mass spectrometry isotope dilution (TIMS-ID) analyses at Cornell.

¶Mean and standard deviation (in percent of mean) of four inductively coupled-plasma mass spectrometry (ICP-MS) analyses at Cornell.

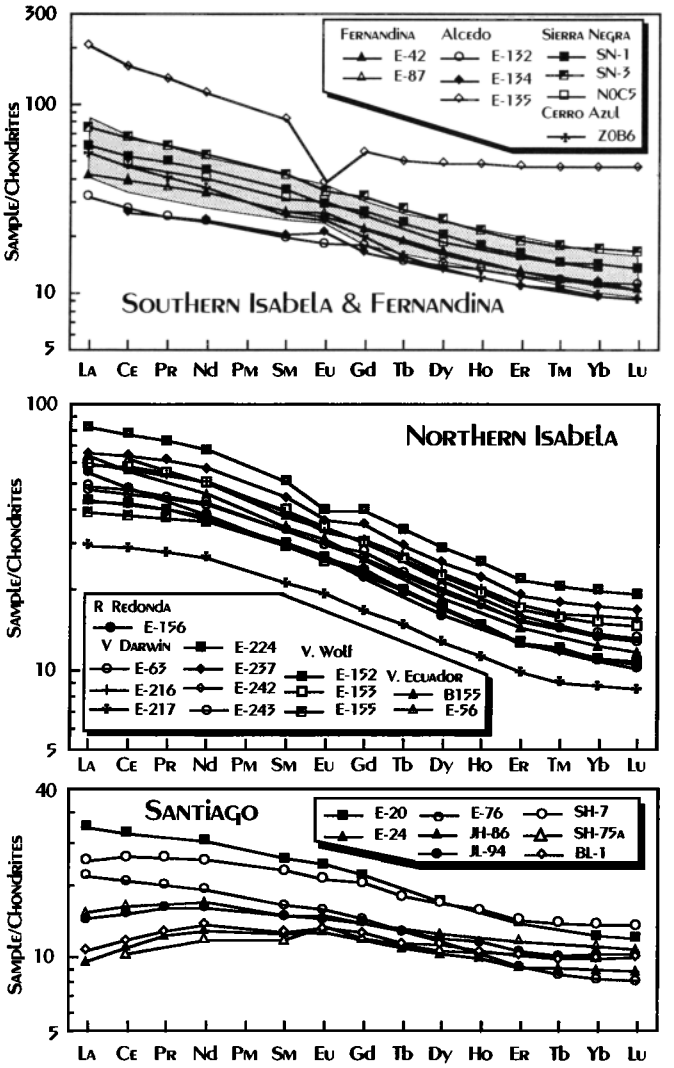

Fig. 9. Chondrite-normalized abundances of rare earths in Isabela, Fernandina and Santiago lavas. Note the parallelism of patterns from Isabela and Fernandina and diversity of patterns from Santiago. Shaded area shows the range of rare earth patterns from Cerro Azul (D. J. Geist, unpublished data, 1992). Chondritic normalizing factors based on the average of 20 ordinary chondrites of *Nakamura* [1974].

Langmuir [1987], then these relationships indicate that isotope ratios, which presumably reflect source compositions, are unrelated to degree of melting.

Finally, both rare earth abundances and $Na_{8.0}$ suggest that magmas of the Santa Cruz shield series have been generated by widely varying extents of melting (Figure 14 and subsequent discussion). Yet the isotopic compositions of these magmas show only limited variations. Indeed, there are no correlations whatsoever between isotope ratios and $Na_{8.0}$, $SiO_{8.0}$, or $Fe_{8.0}$ within individual volcanic suites. These observations are inconsistent with the veined or plum-pudding plume model. Although small-scale hetergeneities probably do exist in the mantle beneath the Galápagos and contribute to local magma variability, we conclude that variable extent of melting of them is not responsible for the large scale patterns observed in Figure 15.

The second model, remelting of the lithosphere, receives some support from the analysis of geophysical observations in the Galápagos by M. A. Feighner and M. A. Richards (submitted manuscript, 1993). The lithosphere appears to be particularly thin under the central part of the archipelago and remelting of the lithosphere is one possible mechanism for this dramatic difference in lithospheric strength. We believe, however, that it is unlikely that remelting of the lithosphere can account for the observed geochemical patterns. *Emerman and Turcotte* [1983] concluded that conduction alone is unlikely to supply sufficient heat to thin the lithosphere above a plume. The only alternative mechanism to conduction is heating by plume-derived melts passing through the lithosphere. It is unlikely that these melts are superheated; thus the energy for heating and melting the lithosphere can be derived only from their crystallization. Since energy for melting is most abundant in direct proximity to conduits and diapirs of these melts, it seems likely that melts produced in the lithosphere will mix with the plume-derived ones.

To evaluate this model, we need to estimate the composition of magmas that could be produced by remelting the lithosphere. As noted, the lithosphere would have gone through extensive melting at the Galápagos Spreading Center. If the melt produced by this process were extracted with 100% efficiency, the residual mantle would be highly depleted. If some melt remained trapped and crystallized in place, the depletion would be less extreme. We considered the case where 1% melt remains trapped in the lithosphere after generation and extraction of a reasonably primitive LREE-depleted MORB (e.g., 5 ppm Nd) by 12% melting.

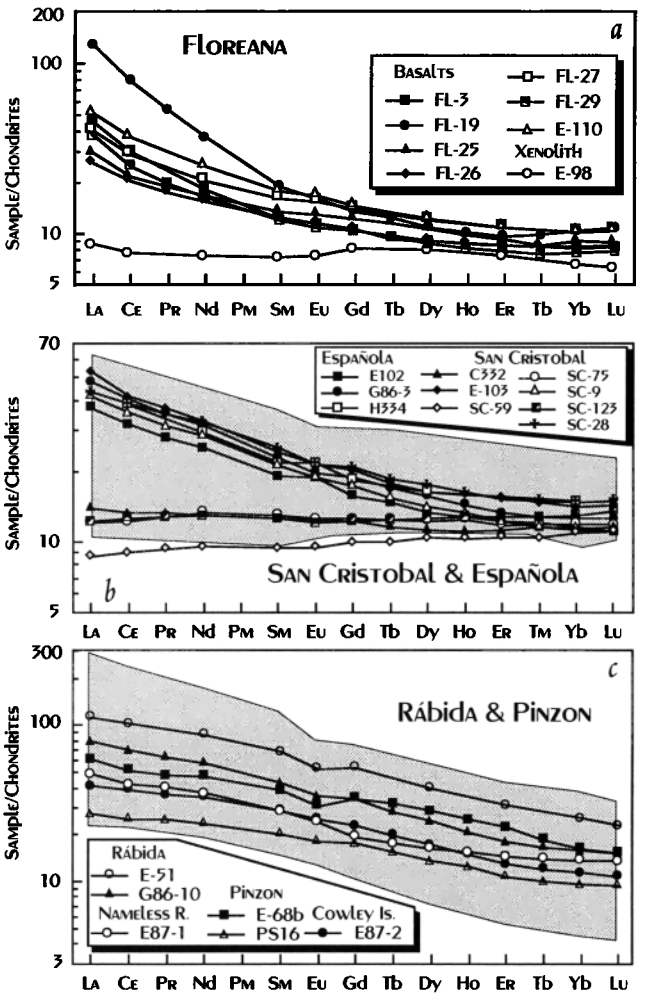

Fig. 10. Chondrite-normalized abundances of rare earths in lavas from the southern islands of Floreana, San Cristobal, and Española and the central islands of Rábida and Pinzón. Shaded area in Figure 10b is the field of San Cristobal rare earth patterns of *Geist et al.* [1985a]. Shaded area in Figure 10c shows the range of rare earth patterns reported by *Shimizu et al.* [1981] from Rábida.

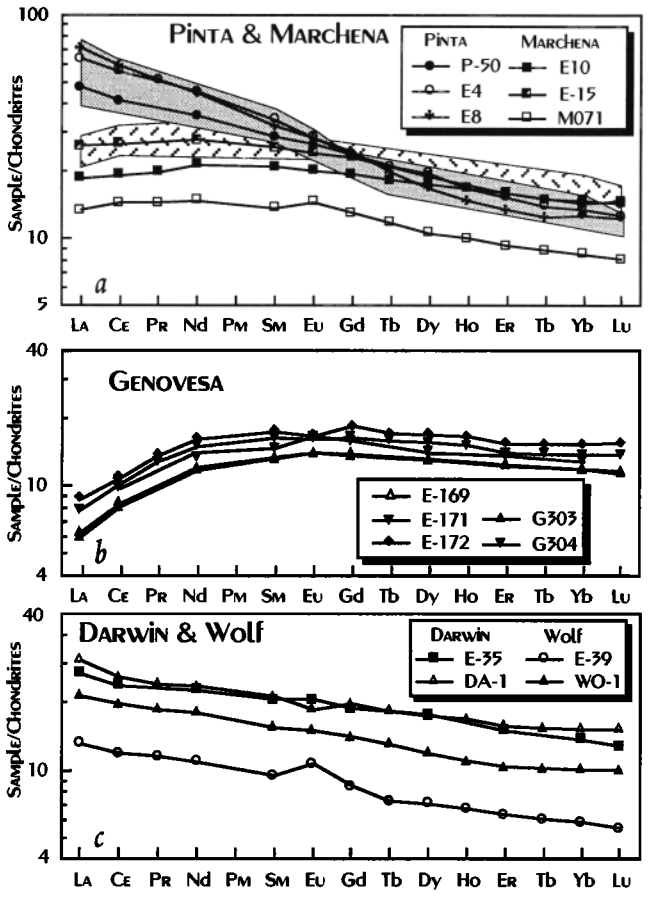

Fig. 11. Chondrite-normalized rare earth patterns of the northern islands of Pinta, Marchena, Genovesa, Darwin, and Wolf. Shaded area in Figure 11c shows the range of rare earth patterns from Marchena determined by *Vicenzi et al.* [1990]; cross-hatched area is the range of rare earths from Pinta reported by *Cullen and McBirney* [1987]. Rare earth patterns from individual volcanos are parallel.

Assuming 5% clinopyroxene in this residue, a 1% "remelt" would have a La/Sm_N ratio of 0.5 and a Nd concentration of 3.7 ppm (higher percent melts would be more depleted). Assuming a primitive plume-derived magma with a composition similar to that of FL-3 ($\varepsilon_{Nd} \approx 5.5$) and that the lithosphere has ε_{Nd} of 10, a 1:1 mixture of remelted lithosphere and plume-derived magma (a more realistic estimate would be 1:10 or 1:100) would have ε_{Nd} of 6.6 and La/Sm_N of 2.6. Assuming 0.1% remelting of the lithosphere or a somewhat more enriched composition (e.g., $\varepsilon_{Nd} \approx 8$) does not substantially change these results. Thus because the lithosphere should be highly depleted, and because any melts produced within it will mix with more enriched plume melts, remelting of the lithosphere cannot produce the magma compositions observed in the central Galápagos. These arguments do not preclude the possibility that heat lost from ascending magma is important in thinning of the lithosphere beneath the central Galápagos; we argue only that this process will have an insignificant effect on isotope and incompatible element ratios or the erupted magmas.

The lithosphere-remelting hypothesis also predicts a specific geographic pattern for those elements sensitive to depth of melting: mean depth of equilibration should be shallowest in the central and northern parts of the plateau where the lithosphere has been thinned. The "missing" lithosphere in the depth region of 6-12 km corresponds to pressures of less than 0.5 GPa. Experimental studies, reviewed by *Klein and Langmuir* [1987], show that melting in this pressure regime should produce magmas dramatically poorer in FeO than those produced in the pressure regime of 0.5-1.5 GPa, which is more typical of MORB production [*Klein and Langmuir*, 1987]. For instance, a 3% melt at 0.5 GPa should have an SiO_2 concentration of about 49% and an FeO concentration of about 6%. This contrasts with mean $Si_{8.0}$ and $Fe_{8.0}$ of 47.6 and 11.4, respectively, for the Santa Cruz shield series. The low SiO_2 and high FeO concentrations of Santa Cruz magmas are very difficult to reconcile with such shallow melting. Thus consideration of the likely melting mechanism, the consequent mixing relationship, and compositional relationships lead us to reject remelting of the lithosphere as a cause of the compositional and isotopic zonations observed.

We conclude that the geographic pattern of isotope and incompatible-element ratios in the Galápagos must reflect large-scale chemical variations in the mantle. *White and Hofmann* [1978] pointed out that the geographic variation in isotope ratios is opposite that predicted by the model of a rising mantle plume mixing radially outward with surrounding depleted asthenosphere, which *Schilling* [1973] proposed to explain geographic variation in rare earth abundances in Iceland and the Reykjanes Ridge. *Geist et al.* [1988] proposed that the geographic pattern results from the Galápagos mantle plume being torus-shaped. This possibility emerges from fluid-dynamic experiments of *Griffiths* [1986] and occurs when the medium surrounding a rising thermally buoyant diapir is conductively heated and entrained by the diapir. The result is a segregated torus of original diapir material surrounding a center of entrained material. *Geist et al.* [1988] argued that in the case of an incompatible element-enriched mantle plume rising through and entraining depleted asthenosphere, the most depleted magmas should erupt above the center of the plume,

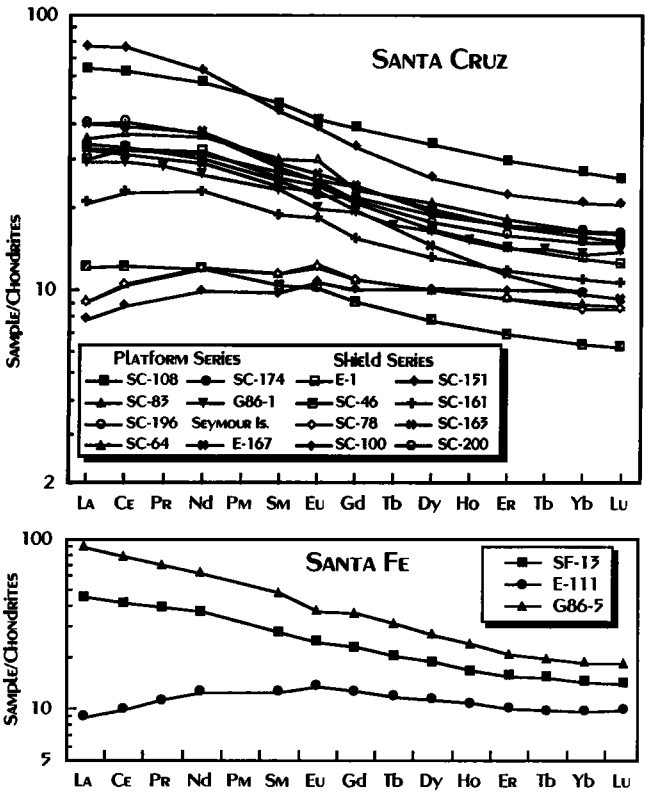

Fig. 12. Chondrite-normalized rare earth patterns of the central islands of Santa Cruz (including Seymour, Baltra, and Las Plazas) and Santa Fe. The diversity of these patterns contrasts with those of the large western volcanos.

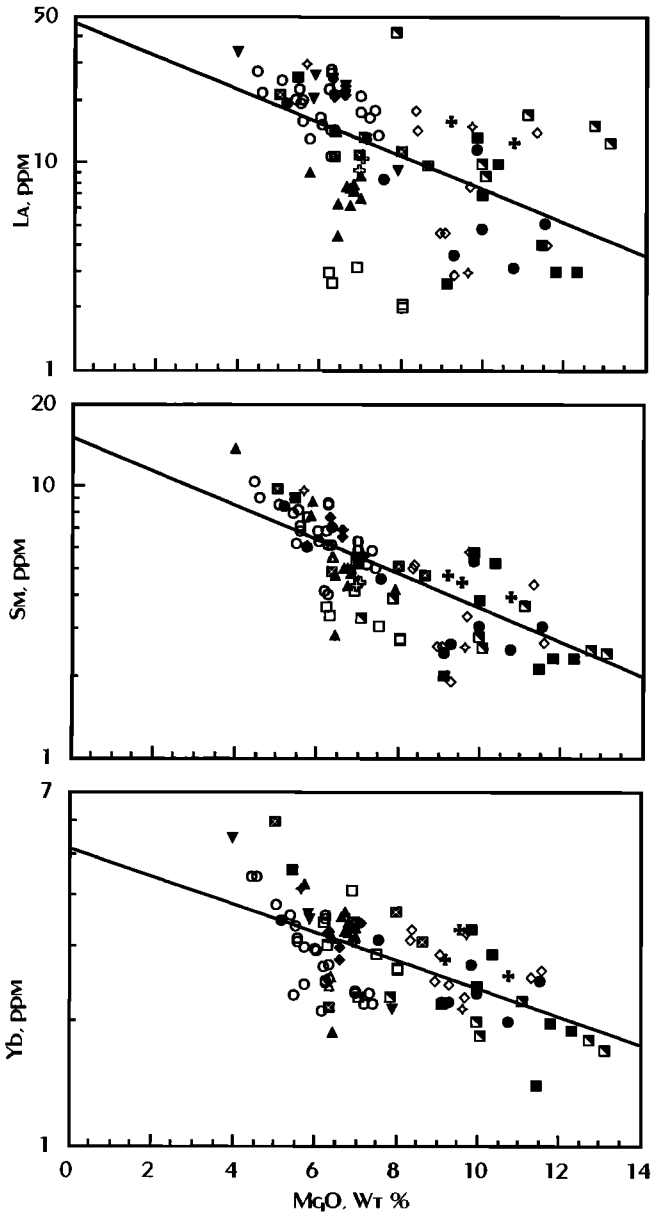

Fig. 13. Abundances of La, Sm, and Yb as a function of MgO in Galápagos lavas. Lines drawn through the data show the slope of the functions used to correct the abundances of the elements to an MgO content of 8%. These equations are $La_{8.0} = La \times e^{0.1827(MgO-8.0)}$, $Sm_{8.0} = Sm \times e^{0.1443(MgO-8.0)}$, $Yb_{8.0} = Yb \times e^{0.07719(MgO-8.0)}$. Rare earth data from *Cullen and McBirney* [1987], *Vicenzi et al.* [1990], *Geist et al.* [1985a], and unpublished data from Cerro Azul of D. J. Geist are also included on this and subsequent figures.

with more enriched ones on the periphery. In a general way, this matches the pattern observed in the Galápagos. *Duncan et al.* [1986] invoked a similar torus-plume model to explain temporal variations in the isotopic compositions of basalts from the Marquesas Islands.

Griffith's [1986] experimental results apply to the transient case of a thermal plume head rather than a continuous plume. The Cocos and Carnegie ridges, however, preserve a record of essentially continuous activity of the Galápagos mantle plume for perhaps the past 25 m.y. Experiments by *Richards and Griffiths* [1989] show that similar toroidial diapirs can be produced by thermal conduit waves resulting from sudden increases in plume flux. Changes in the location of the Galápagos Spreading Center relative to the Galápagos plume complicate the recent volcanic history of the area, so that the plume flux is difficult to estimate. Though a recent increase in plume flux cannot be ruled out, there is little compelling evidence for it.

Another difficulty with this model arises if the plume is subject to shear from horizontal motion of asthenosphere. *Geist et al.* [1985*a*] suggested that the Galápagos plume may be sheared by asthenospheric flow, and this may account for the unusual geochemical patterns in the Galápagos. Experiments by *Richards and Griffiths* [1989] with toroidal diapirs subject to velocity shear show an asymmetric distribution of original diapir material and entrained asthenosphere with the highest concentrations of diapir material "downstream" of the hotspot center. The Nazca plate has moved east-southeast at 37 mm/yr over the last 3 m.y. [*Gripp and Gordon*, 1990], suggesting there should be a significant eastward asthenospheric motion. Shear of the Galápagos mantle plume resulting from this motion would not produce the pattern observed. Thus the torus plume model proposed by *Geist et al.* [1988] encounters substantial, and possibly insurmountable, difficulties.

The same series of fluid dynamical experiments by *Richards and Griffiths* [1989] suggests an alternative, though fundamentally similar, mechanism for entrainment of asthenosphere by the plume. They found that steady state plumes subject to velocity shear will entrain surrounding material in a manner somewhat analogous to that found in the diapir experiments of *Griffiths* [1986]. As the surrounding asthenosphere is conductively warmed by a plume, it becomes thermally buoyant. As the plume is bent by velocity shear, this buoyant asthenosphere becomes entrained in the center, and the original plume material concentrates in the edges and a thin veneer across the top. The result should be a hotspot trace with stripes of "enriched" compositions bounding a central stripe of more depleted material in the center. The idea is illustrated in Figure 16, which shows north-south and east-west cross sections of the bent-plume hypothesis applied to the Galápagos.

The first part of the plume to reach the depth where melting begins is the upper veneer of original plume and entrained asthenosphere beneath it. This melts to produce basalt with moderately enriched trace element and isotopic characteristics, such as that erupting on Fernandina. Farther to the east, melting along the central axis taps entrained asthenosphere with only a small admixture of plume material. Basalt produced in this area will have more depleted signatures, similar to those erupting on Volcan Darwin. Farther along the axis of the plume to the east, melts are derived entirely from this entrained asthenosphere as it crosses the minimum depth for melting, while the original plume material above it becomes exhausted of its basaltic component. Thus along the axis of the plume, the isotopic and trace element signature of the basalts becomes increasingly depleted to the east.

A north-south cross section at the longitude of Isabela shows that volcanos along the axis of the plume, such as Volcan Wolf and Volcan Darwin, tap melts produced primarily by melting of entrained asthenosphere. Alcedo, which sits over the boundary between plume and entrained asthenosphere, has erupted a series of magmas of intermediate isotopic composition that are notably more heterogeneous than those of its northern and southern neighbors. To the north and south, volcanos such as Roca Redonda and Sierra Negra are tapping melts of predominantly original plume material. Though the cartoon in Figure 16 greatly simplifies the situation, we conclude that the $^{87}Sr/^{86}Sr$, ϵ_{Nd}, and La/Sm_N patterns shown in Figure 15 are generally consistent with that expected for melting of a plume bent by velocity shear.

Figure 15 indicates that the plume has a substantial influence

TABLE 6. Volcano Averages

Volcano	$Si_{8.0}$	$Fe_{8.0}$	$Na_{8.0}$	$K_{8.0}$	$^{87}Sr/^{86}Sr$	ε_{Nd}	$^{206}Pb/^{204}Pb$	Ba	$La_{8.0}$	$Sm_{8.0}$	$Yb_{8.0}$	La/Sm_{N8}	Sm/Yb_{N8}
Santa Cruz Platform	47.32	10.42	2.87	0.38	0.70294	7.54	18.769	80.91	10.20	4.99	3.31	1.26	1.64
Santa Cruz Shield	47.65	11.49	3.4	0.38	0.70265	8.64	18.550	43.40	9.66	4.83	2.84	1.24	1.84
Santa Fe	47.66	10.35	3.18	0.65	0.70310	6.83	18.834	195.04	14.45	5.78	3.14	1.54	2.00
Marchena	47.87	10.44	2.96	0.31	0.70281	7.79	18.917	43.28	5.58	3.90	2.94	0.88	1.43
Pinta	47.98	9.74	2.79	0.69	0.70324	5.30	19.238	170.71	15.88	5.49	2.80	1.79	2.12
Genovesa	48.14	10.14	2.75	0.11	0.70269	9.41	18.435	8.91	2.12	2.87	2.90	0.46	1.07
Volcan Ecuador	47.07	9.09	3.06	0.58	0.70311	6.27	19.253	164.00	15.62	5.52	2.44	1.75	2.45
Volcan Wolf	47.36	8.37	2.68	0.37	0.70272	8.11	18.900	60.50	10.43	4.92	2.33	1.31	2.29
Volcan Darwin	47.53	9.39	2.80	0.40	0.70284	7.35	18.778	69.82	11.60	5.30	2.80	1.35	2.05
Volcan Alcedo	47.95	10.28	2.62	0.43	0.70321	6.57	19.216	151.14	9.07	3.63	2.16	1.54	1.83
Sierra Negra	47.04	10.95	2.51	0.58	0.70333	5.55	19.374	128.93	13.53	5.29	2.80	1.58	2.05
Cerro Azul	47.93	9.81	2.90	0.53	0.70334	5.88	19.319	136.50	15.99	5.29	2.33	1.87	2.47
Fernandina	47.43	9.18	2.43	0.29	0.70319	5.92	19.089	82.33	10.30	4.30	2.17	1.48	2.15
San Cristobal	48.45	10.44	2.97	0.61	0.70305	7.78	18.805	69.83	11.45	4.31	3.03	1.64	1.54
Floreana	48.20	10.47	3.34	0.99	0.70348	5.98	19.826	268.48	25.15	4.21	2.39	3.69	1.91
Española	47.40	10.45	2.97	0.59	0.70294	7.63	18.743	87.47	20.08	5.62	3.30	2.20	1.85
Santiago NW	47.01	11.57	2.98	0.45	0.70285	7.36	18.943	47.16	13.53	6.03	3.01	1.39	2.17
Santiago SE	47.39	10.98	2.86	0.34	0.70276	7.99	18.621	18.74	5.45	3.42	2.49	0.98	1.49
Pinzon	47.26	9.97	2.77	0.38	0.70300	7.08	19.018	77.73	11.24	4.90	2.57	1.42	2.07
Rabida	48.50	8.18	3.47	0.78	0.70299	7.05	19.085	163.35	16.94	7.08	3.46	1.48	2.22
Darwin-Wolf	48.96	9.36	2.56	0.29	0.70309	6.43	19.053	65.66	8.08	3.75	3.00	1.33	1.35

$Na_{8.0}$, $Si_{8.0}$, $K_{8.0}$, and $Fe_{8.0}$ are the concentrations of Na_2O, SiO_2, K_2O, and ΣFeO corrected for fractional crystallization to the equivalent of 8% MgO [*Klein and Langmuir*, 1987]. Lavas that were obviously cumulates, those with <5% MgO, and those with >13% MgO were not used in computing $Na_{8.0}$, $Si_{8.0}$, and $Fe_{8.0}$. Corrections were made using the equations of *Geist* [1992], which are for MgO>9% (olivine only saturated); $Y_{8.0} = Y + a(MgO-9) + b$; and for MgO<9% (multiply saturated); $Y_{8.0} = Y + b(MgO-8)$. For the volcanoes of Isabela and Fernandina as well as Pinta and Rábida, $b_{Na} = 0.114$, $b_{Si} = 0.471$, $b_{Fe} = 1.21$, $b_K = 0.571$, and a was not applicable. For the remaining volcanoes, $b_{Na} = 0.211$, $b_{Si} = 0.625$, $b_{Fe} = 0.678$, $b_K = 0.139$; $a_{Na} = 0.0687$, $a_{Si} = 0.282$, $a_{Fe} = 0.0153$, and $a_K = 0.0115$.

on the geochemistry of the mantle beneath the GSC, as *Schilling et al.* [1976] previously observed. *Verma et al.* [1982] and *Morgan* [1978] suggested that flow of the plume to the ridge was channeled at shallow levels beneath the Wolf-Darwin Lineament. Indeed, *Morgan* [1978] suggested the Wolf-Darwin Lineament was the manifestation of this shallow flow. However, Figure 15 suggests the flow occurs over a much broader area. Furthermore, *Harpp et al.* [1990] found that isotope ratios in basalts dredged from the Wolf-Darwin Lineament become more plume-like toward the GSC. This observation is not obviously predicted by the channelized shallow flow hypothesis.

The most plume-like isotope ratios on the GSC occur near it's intersection with the Wolf-Darwin Lineament [*Verma and Schilling*, 1982; *Verma et al.*, 1983] northwest of the archipelago. This requires plume flow in a direction nearly opposite to the absolute motion of the Nazca plate, and presumably the shallow asthenosphere, since the latter's motion is undoubtedly viscously coupled to the overlying plate. We suggest that a possible solution to this dilemma is flow of plume material to the ridge at a much deeper level, perhaps related to deep asthenospheric counterflow toward the ridge.

Degree and Depth of Melting

Degree and depth of melting can be assessed from a consideration of rare earth and Nd isotope systematics. Figure 17a shows ε_{Nd} plotted against $[La/Sm]_{N8.0}$. The two are correlated, as would be expected from plume–asthenosphere mixing. There is nonetheless considerable scatter, which can be modeled as variable extents of partial melting superimposed on this mixing. The simple calculations shown in Figure 17 illustrate this.

A partial melt will have higher La/Sm than its source, and hence any ε_{Nd}–La/Sm curve for mixing between sources should define the minimum La/Sm ratio observed in basalts with a given ε_{Nd}. We constructed a binary mixing model based on this observation and on the maximum and minimum observed ε_{Nd}.

TABLE 7. Correlation Matrix for Volcano Averages

	$^{87}Sr/^{86}Sr$	ε_{Nd}	$^{206}Pb/^{206}Pb$	$La/Sm_{N8.0}$	$Sm/Yb_{N8.0}$	Ba	$La_{8.0}$	$Sm_{8.0}$	$Yb_{8.0}$	$Si_{8.0}$	$Fe_{8.0}$	$Na_{8.0}$	$K_{8.0}$
$^{87}Sr/^{86}Sr$	1.00												
ε_{Nd}	-0.90*	1.00											
$^{206}Pb/^{206}Pb$	0.88*	-0.85*	1.00										
$La/Sm_{N8.0}$	0.71*	-0.56*	0.75*	1.00									
$Sm/Yb_{N8.0}$	0.38†	-0.55*	0.50†	0.38†	1.00								
Ba	0.80*	-0.71*	0.80*	0.78*	0.49†	1.00							
$La_{8.0}$	0.62*	-0.56*	0.66*	0.90*	0.60*	0.79*	1.00						
$Sm_{8.0}$	0.14	-0.31	0.19	0.24	0.73*	0.39†	0.62*	1.00					
$Yb_{8.0}$	-0.31	0.31	-0.41†	-0.19	-0.31	-0.14	0.05	0.41†	1.00				
$Si_{8.0}$	0.17	-0.01	0.10	0.10	-0.43†	0.15	-0.03	-0.26	0.20	1.00			
$Fe_{8.0}$	-0.10	0.20	-0.19	0.01	-0.36	-0.20	-0.10	-0.23	0.13	-0.27	1.00		
$Na_{8.0}$	-0.11	0.22	0.00	0.33	0.13	0.35	0.45†	0.43†	0.40†	0.17	0.12	1.00	
$K_{8.0}$	0.63*	-0.53†	0.66*	0.83*	0.45†	0.86*	0.90*	0.55*	0.12	0.15	-0.06	0.57*	1.00

Values are based on 124 analyses averaged among 21 volcanic centers. Darwin and Wolf Islands were combined in a single average. Lavas from Santiago were divided between northwest and southeast, those from Santa Cruz were divided between Platform and Shield series.

*Correlations significant at the 0.5% level.

†Correlations significant at the 5% level.

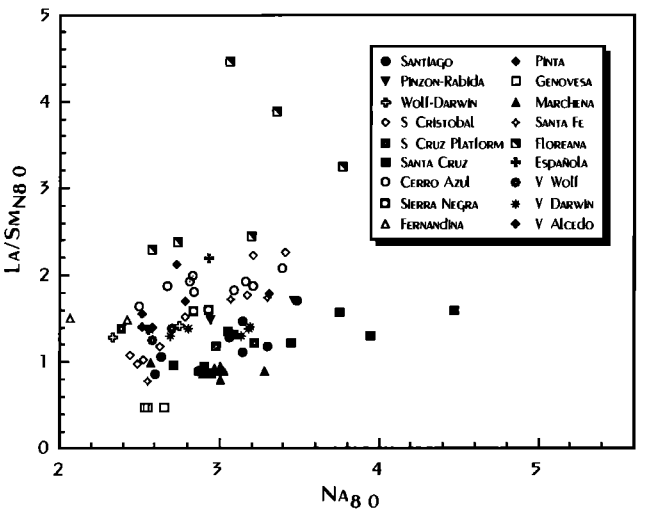

Fig. 14. Variation of $La/Sm_{N8.0}$ with $Na_{8.0}$ in Galápagos lavas. Although there is no overall correlation, there are apparent within-suite correlations for Santa Cruz shield, Santiago, San Cristobal, Cerro Azul, and perhaps Santa Fe. These correlations are consistent with the predicted effects of variable extent of partial melting.

The compositions of the depleted asthenospheric and enriched plume components, which are based on these criteria, are given in the caption to Figure 17. We then calculated the effects of equilibrium partial melting of this mixture. While the absolute degrees of melting are arbitrary and depend on the choice of mantle components, Figure 17a nevertheless allows comparison of relative degrees of melting. In general, the northern (Marchena, Genovesa, Pinta, Wolf, and Darwin) and western volcanos, particularly Fernandina and Sierra Negra, are the products of the largest degrees of melting. The least melting occurs under Santa Cruz and the southern islands of Floreana, Española, and San Cristobal. Figure 17 also indicates that degree of melting under these islands, particularly Santa Cruz, Floreana, and San Cristobal, has been quite variable.

These conclusions, however, are based on our assumption of simple binary mixing. As we discuss below, there is evidence that the plume itself is laterally heterogeneous. Our mixing model is based on compositions appropriate for the northern islands, which may not be appropriate for the southern islands, particularly San Cristobal and Floreana. It is possible, therefore, that lavas from these islands are generated by larger degrees of melting than suggested by Figure 17. We have also assumed constant distribution coefficients in our modelling. However, *Gallahan and Nielsen* [1992] have demonstrated a systematic dependence of clinopyroxene rare earth partition coefficients on temperature and melt composition. The result of these dependencies is that partition coefficients decrease with increasing extent of melting. The use of variable partition coefficients would allow production of high La/Sm melts by slightly greater degrees of melting than those implied by Figure 17.

Figure 17b shows $Sm/Yb_{N8.0}$ plotted against $La/Sm_{N8.0}$. Also shown is the same mixing curve as in Figure 17a. Because garnet strongly fractionates Sm and Yb during melting whereas clinopyroxene, the only other mantle phase accepting significant amounts of the rare earths, does not, the Sm/Yb ratio should be particularly sensitive to the presence or absence of garnet and therefore to depth of melting. Thus we have calculated separate melting curves for garnet and spinel peridotite (we have not specifically considered melting of plagioclase peridotite, which will produce fractionations similar to, but less pronounced than, spinel peridotite melting). As may be seen, melting of garnet peridotite produces strong enrichment of Sm over Yb in the melt, whereas melting of spinel peridotite does not. Most Galápagos basalts, particularly those from Marchena, Santa Cruz, Santiago, Fernandina, and most of the Isabela volcanos, have high Sm/Yb ratios, implying that they were generated primarily in the garnet stability field. Basalts from the southern islands, particularly those from Floreana and San Cristobal, have lower Sm/Yb ratios, indicating they were produced primarily in the spinel stability field. *Bow* [1979] and *Bow and Geist* [1992] also concluded that Floreana magmas were produced within the spinel stability field, whereas *Geist et al.* [1985*a*] concluded San Cristobal magmas were produced within the garnet stability field (however, D. J. Geist (personal communication, 1992) now agrees that San Cristobal magmas were derived primarily within the spinel stability field). Darwin and Wolf islands also appear to be products of relatively shallow melting.

When ε_{Nd}, La/Sm, and Sm/Yb are considered simultaneously, most Galápagos basalts cannot be modeled as melts of either just garnet peridotite or just spinel peridotite. They are more likely the products of polybaric melting that begins in the stability field of garnet and ends in that of spinel, which is expected for a rising mantle diapir. *Salters and Hart* [1989] found such polybaric melting necessary to explain Lu-Hf and Sm-Nd systematics in MORB. Figure 17 also shows calculated melting paths for three examples of "progressive melting". In each case, 1% batch melts were produced, extracted, and pooled; the curves show the composition of the pooled melts. In curve *A*, the first 6% melting (i.e., first six increments) occurs in the garnet stability field, with the remainder in the spinel stability field. In curves *B* and *C*, the first 2% and 1% melt increments, respectively, occur in the garnet stability field, and all subsequent melts form in the spinel stability field. These examples of progressive melting show that rare earth patterns retain the signature of garnet even if only a small percentage (10-20%) of the total melting occurs in the garnet stability field. This is because a relatively large fraction of the incompatible elements are extracted in the earliest melting increments. These early melting increments therefore dominate the incompatible element budget of the pooled melts. These calculations thus reinforce the conclusion that some of the Floreana, Española, and San Cristobal magmas must have been produced at shallow depth as they retain no garnet signature whatsoever.

The inferences on degree and depth of melting derived from rare earth and Nd isotope relationships in Figure 17 are generally consistent with variations in $Si_{8.0}$, $Na_{8.0}$, and $Fe_{8.0}$, though there are some differences. For example, the high $Na_{8.0}$ values for lavas from Floreana, Santa Cruz, Española, and San Cristobal are consistent with low degrees of melting inferred from ε_{Nd}–La/Sm_N systematics. Lowest $Na_{8.0}$ values occur in in the western and northern part of the archipelago, implying the greatest degrees of melting, and highest mantle temperatures, in those areas. Again, this is consistent with the inference we made above from ε_{Nd}–La/Sm_N systematics. Low $Fe_{8.0}$ in the southern island lavas implies rather shallow melting, consistent with the low Sm/Yb_N ratios. The high $FeO_{8.0}$ ratios for Santa Cruz and Santiago suggest deeper melting beneath the center of the archipelago, as do Sm/Yb-La/Sm systematics. However, low $Fe_{8.0}$ for lavas from Fernandina and the Wolf and Ecuador volcanos of northern Isabela suggests shallow melting, yet these lavas generally have high Sm/Yb, indicative of melting in the garnet stability field. The discrepancy may reflect the observation we made above, namely, that incompatible element abundances in pooled

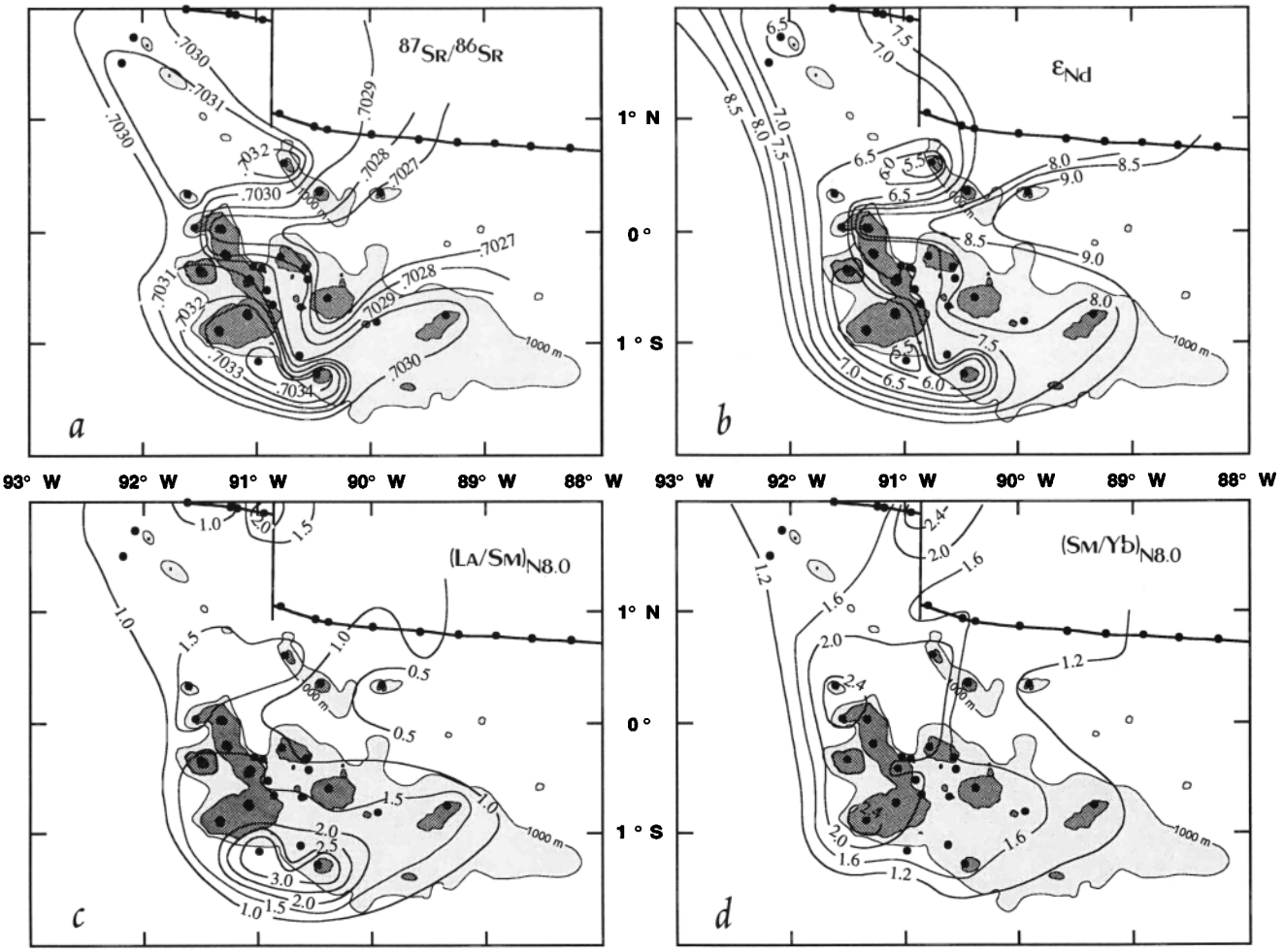

Fig. 15. Computer generated contours of (a) $^{87}Sr/^{86}Sr$, (b) ε_{Nd}, (c) $La/Sm_{N8.0}$, and (d) $Sm/Yb_{N8.0}$ in the Galápagos Archipelago and adjacent GSC, the latter with the data of *Schilling et al.* [1982], *Verma and Schilling* [1982], and *Verma et al.* [1983]. Contouring was based on averages for individual volcanos for the islands and individual samples for the GSC. Locations were corrected for plate motion to the position occupied at the average eruption time. Two averages were computed for Santiago because of systematic differences in composition between the northwest and southeast. Two averages, with lavas grouped by age, were also computed for Floreana, San Cristobal, and Santa Cruz.

progressive or "sequential" melts are controlled by earlier melting increments, but this is not the case for compatible elements such as iron. On the other hand, our data for these volcanos are sparse, and hence we have little confidence in the low average $Fe_{8.0}$.

It is interesting to compare our inferences on depth and degree of melting with the structure inferred by M. A. Feighner and M. A. Richards (submitted manuscript, 1993). We conclude melting is shallow and of relatively small degree beneath Floreana and Española, which seems consistent with the thicker lithosphere (implying cooler temperatures) and thinner crust inferred by M. A. Feighner and M. A. Richards (submitted manuscript, 1993). They find the crust to be quite thick beneath the central archipelago, particularly eastern Isabela, where it appears to reach a total thickness of 18 km. From our inferences, we would expect most crustal thickening to occur in the west, in the area of Fernandina and Isabela, where degree of melting is largest. The thick crust M. A. Feighner and M. A. Richards (submitted manuscript, 1993) find in the central platform was apparently produced when that lithosphere was farther to the west. Relatively smaller degree melts erupted on the central platform (i.e., on Santa Cruz) would result in comparatively minor additional crustal thickening.

On the whole, Galápagos lavas have similar Na_2O, lower SiO_2, and slightly higher FeO than do MORB at similar MgO concentration (Figure 2). This suggests that the degree of melting beneath the Galápagos is similar to that beneath mid-ocean ridges but that the depth of melting is somewhat greater (assuming the plume and asthenosphere have similar major element compositions). The similarity in degree of melting is somewhat surprising, given the high inferred temperatures beneath the Galápagos [*Schilling*, 1991]. We note, however, that both Fernandina and Sierra Negra seem to have less Na_2O than average MORB. This suggests that the plume component is indeed hotter than the asthenosphere beneath ridges. The lower temperatures elsewhere in the Galápagos may reflect conductive heat loss from the plume to the surrounding asthenosphere.

We pointed out earlier that Galápagos lavas have more Na_2O and less SiO_2 and ΣFeO than Kilauean lavas, which implies lower degrees of melting, and perhaps greater depths of melting beneath the Galápagos (assuming the Hawaiian and Galápagos plumes have similar major element compositions). The lower degree of melting is consistent with the apparent lower excess temperature estimated for the Galápagos (215°C; [*Schilling*, 1991]) than for Hawaii (300°C; [*Wyllie*, 1988]), but these lower temperatures should result in shallower melting than in Hawaii, which is not consistent with the lower SiO_2 and ΣFeO of the Galápagos.

The inferred variations in depth and degree of melting are

broadly consistent with the sheared plume model outlined above, with highest mantle temperatures above the ascending limb of the plume in the west, and lower temperatures to the south, east, and north. Superimposed on this pattern appears to be a general trend of decreasing degree and depth of melting southward. This strongly suggests a tendency toward cooler mantle temperatures to the south, away from the spreading center. That mantle temperatures should decrease away from the spreading center is, of course, quite reasonable. We were nevertheless surprised that this cooling is observable even in the presence of the Galápagos plume, which has an excess temperature of 215°C according to *Schilling* [1991]. This implies that the asthenosphere has a strong thermal influence on the plume, apparently drawing heat from it. The strong thermal interaction between plume and asthenosphere is consistent with the entrainment of thermally buoyant asthenosphere by sheared plumes as proposed by *Richards and Griffiths* [1989].

Heterogeneity Within the Plume

In the discussion above, we assumed that the mantle source of Galápagos magmas is a mixture of two homogenous components: the plume and depleted asthenosphere. The isotope data, however, suggest a subtle compositional difference between the north and south limbs of the plume. For example, although Floreana and Pinta have similar ε_{Nd} values, Floreana has higher $^{87}Sr/^{86}Sr$ (Figures 6 and 14). Lavas from San Cristobal in the south define the high $^{87}Sr/^{86}Sr$ side of the $^{87}Sr/^{86}Sr$–ε_{Nd} Galápagos array, while the northern volcanos, such as Marchena, Wolf Island, Darwin Island, Volcan Wolf, and Volcan Darwin, define the low $^{87}Sr/^{86}Sr$ side of the array. These north-south differences are illustrated in Figure 18. The southern Isabela volcanos, Cerro Azul and Sierra Negra, plot between the Floreana and Pinta fields. A somewhat similar north-south variation is apparent in the ε_{Nd}–$^{206}Pb/^{204}Pb$ array (Figure 8). In Figure 7, the northern islands of Pinta, Wolf, and Darwin have distinctly higher $^{207}Pb/^{204}Pb$ and $^{208}Pb/^{204}Pb$ for a given $^{206}Pb/^{204}Pb$ than the remaining islands.

These north-south differences are most apparent in lavas with the most enriched signatures and are orthogonal to the main arrays in isotope ratio diagrams (Figure 18). They are, therefore, not readily explained by plume-asthenosphere mixing. We conclude that these differences reflect lateral heterogeneity in the plume itself, perhaps intrinsic to the deep mantle source of the plume. In this respect, the Galápagos seem volcanos somewhat analogous to Hawaiian ones. The emergent volcanos of the Hawaiian chain appear to be arranged in two chains, "Loa" and "Kea". While arrangement of volcanos in these chains appears to reflect lithospheric stresses [*Moore*, 1987], systematic differences in isotopic composition [e.g., *Stille et al.*, 1986] suggest lateral heterogeneity in the Hawaiian plume.

Major Element Patterns and Crustal Processes

Figure 17 shows that some volcanos (Marchena and Fernandina, for example) appear to erupt products of a relatively uniform degree of melting, while others (Santa Cruz and Floreana, for example) erupt basalts produced by a wide range of melting. The apparently uniform extents of melting in the former group, which also includes Pinta, Genovesa, and the large volcanos of Isabela, could reflect either uniform melting or homogenization of diverse melting products in central magma chambers. The volcanos of this group also have, for the most part, relatively uniform major element and isotopic compositions and Mg#. This suggests to us that magma chambers beneath these islands are serving to homogenize melts passing through them.

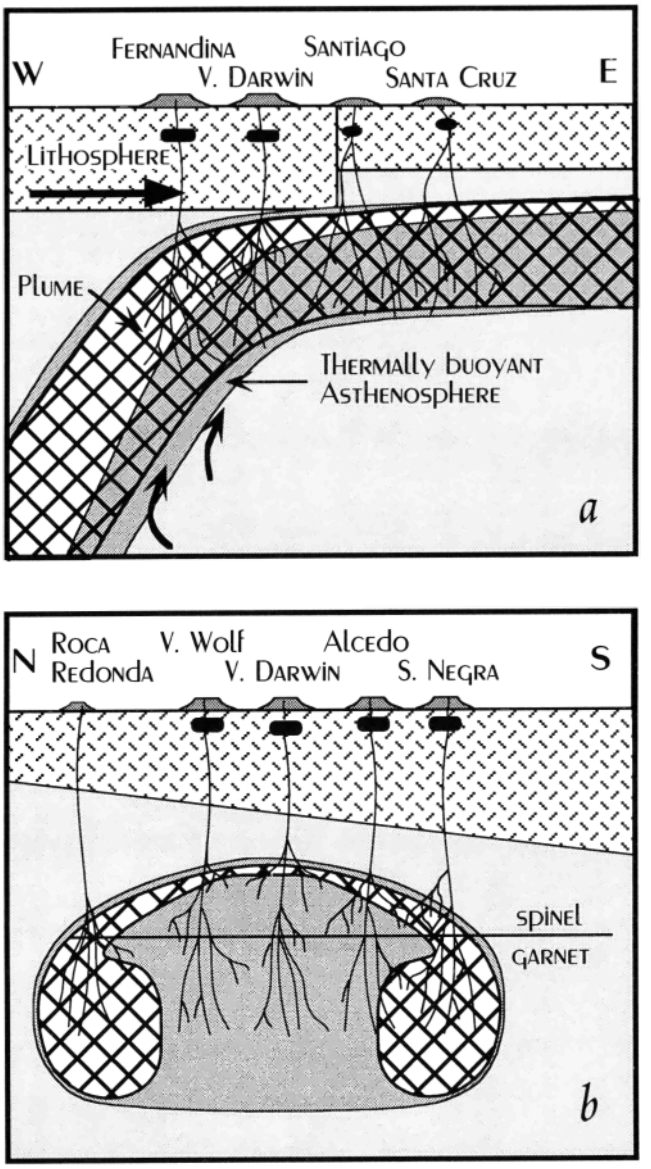

Fig. 16. Cartoon illustrating the sheared plume model. Stippled pattern represents lithosphere, cross-hatched pattern is original plume material, grayed patterned is asthenosphere, darker gray is thermally buoyant asthenosphere. (a) East-west cross section beneath the center of the archipelago; (b) north-south cross section at the longitude of Isabela.

A related feature is a decrease of minimum Mg# for a volcano toward the center of the archipelago and the restriction of the most differentiated lavas to the west central volcanos. Since Mg# is effectively insensitive to degree of melting, this distribution must reflect shallow level fractional crystallization. The most differentiated lavas occur near the center of the plume and overlap the area where $Na_{8.0}$ indicates that the degree of melting is highest.

We believe this distribution reflects a combination of several factors: magma supply rates (which in turn determine whether permanent magma chambers can be maintained), a tendency for large central volcanos to evolve toward production of differentiated lavas as they age and magma supply wanes, and relatively old and cool lithosphere. We argue that eruption of differentiated lavas can occur only where magma supply rates are high enough to sustain a permanent crustal magma chamber. The observation of *Sinton and Detrick* [1992] that magmas from the

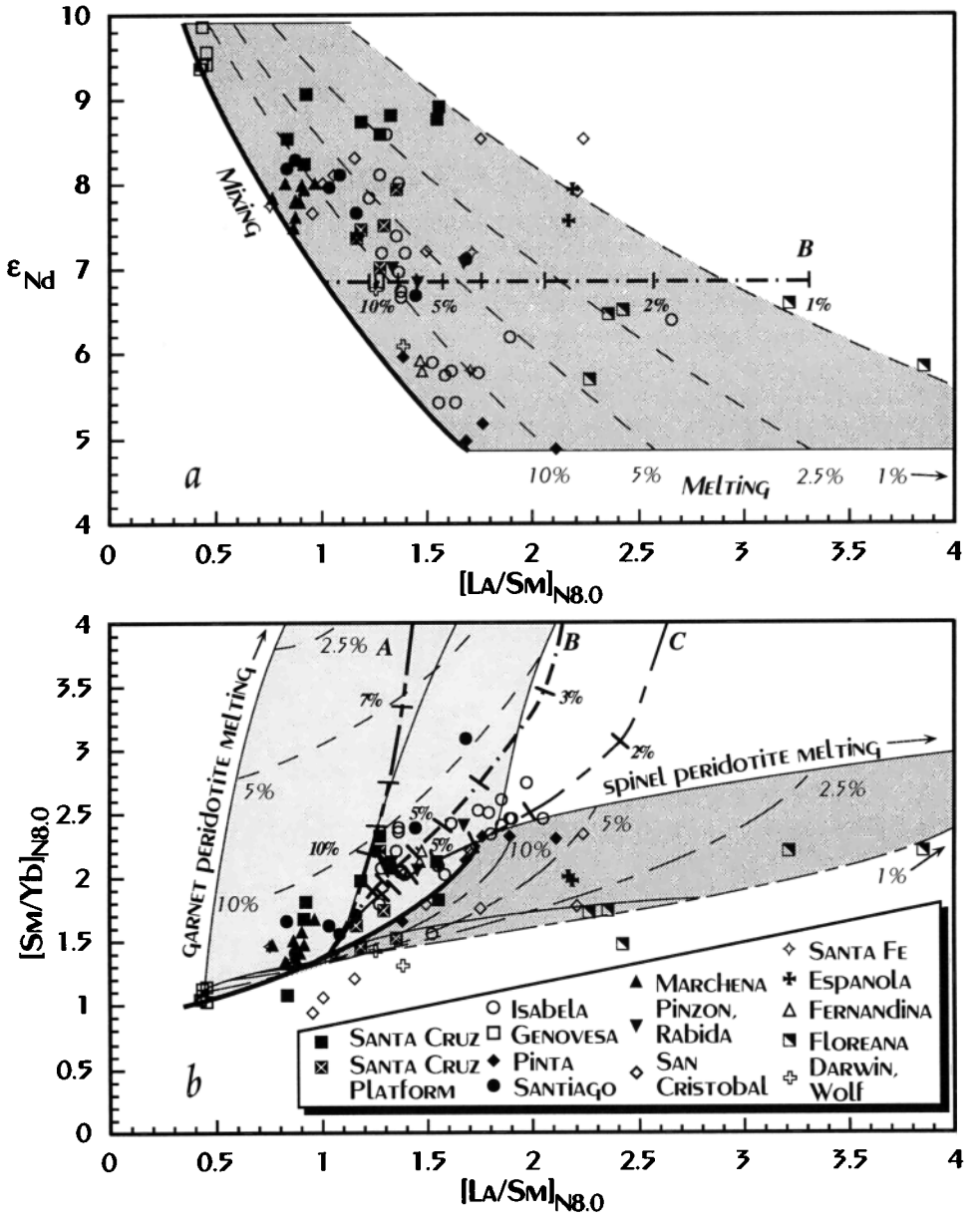

Fig. 17. (a) ε_{Nd} and (b) $[Sm/Yb]_{N8.0}$ plotted against $[La/Sm]_{N8.0}$. Heavy solid line is a hypothetical plume-asthenosphere mixing curve. The "depleted asthenosphere" end-member has $\varepsilon_{Nd} = 9.8$, $La/Sm_N = 0.35$, $Sm/Yb_N = 1$; the "enriched plume" end-member has $\varepsilon_{Nd} = 4.85$, $La/Sm_N = 1.7$, $Sm/Yb_N = 2.2$, Nd concentration 3.45 times higher than in the depleted source. Finer lines illustrate equilibrium partial melting of this mixture. Fine dashed lines represent constant melt fractions (1%, 2.5%, 5%, and 10%). In Figure 17b the effects of melting in the garnet and spinel peridotite stability fields are compared. Garnet strongly fractionates Sm from Yb and melting of garnet peridotite consequently produces a much higher Sm/Yb ratio in the melt. Also shown are the calculated paths for three examples of polybaric progressive melting (dashed curves labeled *A*, *B*, and *C*). In each case, 1% melting increments are produced, extracted, and pooled. The first 6%, 2%, and 1% of melting occur in the garnet stability field for curves *A*, *B*, and *C*, respectively, with subsequent melting occurring in the spinel stability field. The curves show how the composition of the pooled melt changes with increasing total degree of melting.

fast spreading East Pacific Rise are, on average, more differentiated than those of the slow spreading Mid-Atlantic Ridge supports this hypothesis. If magma supply rate is low, magma remaining in the crust after an eruptive episode crystallizes in place before the new magma is injected. At higher rates of production, large pools of magma remain in the crust, cooling and crystallizing, and mix with the next batch of magma arriving from the mantle. When magma supply eventually wanes, this mixing ratio increasingly favors the remaining differentiated melt. Rábida and Pinzón seem to have passed through such a stage. Several of the large western volcanos may eventually reach this stage, but at present, only Alcedo, which has erupted a bimodal rhyolite-basalt suite over the past 100 kyr or so, is currently in it. Santiago apparently also passed through such a phase but now appears to be experiencing a rejuvenation. The uniform compositions of Pinta, Marchena, and Genovesa suggest that these volcanos are also underlain by permanent magma chambers, though they have not erupted highly differentiated lavas. Either they have not yet reached this phase of their evolution, or the young, warm nature of the lithosphere in this area limits cooling and fractional crys-

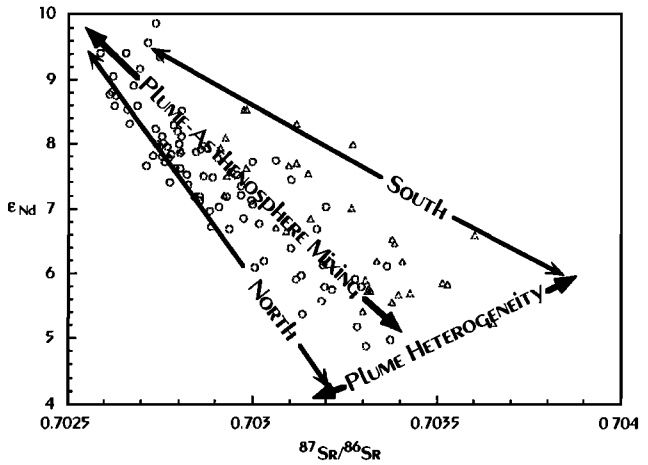

Fig. 18. ε_{Nd} plotted against $^{87}Sr/^{86}Sr$ to illustrate how both plume–asthenosphere mixing and north-south heterogeneity within the plume appear to be required to explain the total isotopic variation in Galápagos lavas. Data from Genovesa, Marchena, Pinta, Wolf Island, Darwin Island, Santiago, Santa Cruz, Santa Fe, Volcan Ecuador, Volcan Wolf, Volcan Darwin, Fernandina, Pinzon, and Rábida (the "Northern Volcanos") are plotted as open circles; data from the southern volcanos (Volcan Alcedo, Cerro Azul, Sierra Negra, Floreana, Española, and San Cristobal) are plotted as open triangles. The southern volcanos generally have higher $^{87}Sr/^{86}Sr$ for a given ε_{Nd}.

tallization. M. A. Feighner and M. A. Richards (submitted manuscript, 1993) noted that the occurrence of highly differentiated lavas seems restricted to the region of thickest crust. Since thick crust requires high magma supply rates, this observation is consistent with the explanation we propose here. Alternatively, thick crust may result in magma ponding at relatively great depth (due to lack of density contrast), where it can cool and crystallize slowly until its density decreases sufficiently that it can rise to the surface.

Conclusions

The most important observation made here is that isotope and incompatible element ratios define a horseshoe pattern with the most depleted signatures in the center of the Galápagos Archipelago and the more enriched signatures on the eastern, northern, and southern periphery. We suggest that this reflects thermal entrainment of asthenosphere by a mantle plume undergoing velocity shear. Alternative hypotheses, such as progressive melting of a veined mantle or remelting of lithosphere beneath the center of the archipelago, predict relationships between major and trace elements and isotope ratios that are inconsistent with those actually observed.

Superimposed on the source variations produced by entrainment of asthenosphere are both heterogeneity within the plume itself and regional variations in degree and depth of melting. The plume appears to be laterally heterogeneous in a north-south direction, with the southern limb having higher $^{206}Pb/^{204}Pb$ and $^{87}Sr/^{86}Sr$ and possibly La/Sm for a given ε_{Nd}. The lack of correlation between isotope ratios and $Na_{8.0}$, $Si_{8.0}$, and $Fe_{8.0}$ indicates that neither degree nor depth of melting affect the isotope ratios of Galápagos magmas. It also indicates that whatever differences in Na_2O, SiO_2, and FeO there might be between plume and asthenosphere, they are very much secondary to the effects of degree and depth of melting on the latter. Incompatible trace element ratios, after correction for the effects of fractional crystallization, reflect variations in both source composition and degree and depth of melting.

Both major and trace element abundances suggest that the greatest degree of melting occurs beneath the central western volcanos. Degree of melting decreases eastward and to the north and south. This pattern suggests that interaction between the plume and the surrounding asthenosphere results in significant cooling of the plume. Superimposed on this thermal pattern produced by plume-asthenosphere interaction is a tendency for melting to be less extensive and to occur at shallower depths to the south, presumably reflecting a decrease in ambient asthenospheric temperature away from the GSC. Magmas erupted on the southern islands are produced primarily by melting in the spinel stability field, while those erupted on the central and northern islands are produced primarily in the garnet stability field. The greatest depth of melting may occur beneath the central islands of Santa Cruz and Santiago.

Overall, our results suggest that the Galápagos mantle plume interacts strongly with the asthenosphere. This extensive interaction appears to be unique among oceanic island groups. We suspect that this reflects the special tectonic setting of the Galápagos. The plume emerges beneath young lithosphere adjacent to a moderately fast spreading ridge, but absolute plate, and presumably shallow asthenospheric, motion is almost parallel to the ridge. More work on the dynamic and thermal interaction of plumes with the asthenosphere is needed before a full understanding of the Galápagos can be achieved.

Acknowledgments. We thank Mike Cheatham and Christine McBirney for performing many of the major and trace element analyses reported here and Mike Cheatham and Karen Harpp for proofreading the manuscript. The work benefited immensely from discussions with our colleagues and coconspirators Dave Christie, Mark Richards, Dennis Geist, Mark Feighner, Ross Griffiths, and Karen Harpp. We also thank Denny Geist and Tom Simkin for providing additional samples and for access to their unpublished data and the Darwin Research Station for assistance with field work. Thanks as well to Stan Hart, Denny Geist, and Karen Harpp for their helpful comments on an early version of this manuscript. Formal reviews by Jamie Allen, Stan Hart, Emily Klein, and Tom Simkin resulted in substantial improvements to the manuscript. This work was supported by NSF grants INT-8315432, EAR85-07973, and OCE89-15402 to A.R.M.; EAR85-20704 to W.M.W. and RAD; OCE89-17031 to W.M.W.; and OCE89-11286 to R.A.D.

References

Bailey, K., Potassium-argon ages from the Galápagos Islands, *Science*, *192*, 465-467, 1976.

Baitis, H., Geology, petrography, and petrology of Pinzón and Santiago islands, Galápagos Archipelago, Ph.D. dissertation, Univ. of Oreg., Eugene, 1976.

Baitis, H. W., and M. Lindstrom, Geology, petrography, and petrology of Pinzón Island, Galápagos Archipelago, *Contrib. Mineral. Petrol.*, *72*, 367-386, 1980.

Baitis, H. W., and F. J. Swanson, Ocean rise-like basalts within the Galápagos Archipelago, *Nature*, *259*, 195-197, 1976.

Batiza, R., and D. Vanko, Petrology of young Pacific seamounts, *J. Geophys. Res.*, *89*, 11,235-11,260, 1984.

Bow, C. S., Geology and Petrogenesis of lavas from Floreana and Santa Cruz islands, Galápagos Archipelago, Ph.D. dissertation, 308 pp., Univ. of Oreg., Eugene, 1979.

Bow, C. S., and D. J. Geist, Geology and petrology of Floreana Island, Galápagos Archipelago, Ecuador, *J. Volcanol. Geotherm. Res.*, *52*, 83-105, 1992.

Brown, J., A. Colling, D. Park, J. Phillips, D. Rothery, and J. Wright, *Seawater: Its Composition, Properties and Behavior*, 165 pp., Pergamon, New York, 1989.

Cassignol, C., and P.-Y. Gillot, Range and effectiveness of unspiked potassium-argon dating: Experimental groundwork and applications, in *Numerical Dating and Stratigraphy*, edited by G. S. Odin, pp. 159-179, John Wiley and Sons, New York, 1982.

Chadwick, W. W., and K. A. Howard, The pattern of circumferential and radial eruptive fissures on the volcanos of Fernandina and Isabela islands, Galápagos, *Bull. Volcanol., 53*, 259-275, 1991.

Chadwick, W. W. J., T. De Roy, and A. Carrasco, The September 1988 intracaldera avalanche and eruption at Fernandina volcano, Galápagos Is., *Bull. Volcanol., 53*, 276-286, 1991.

Cheatham, M. M., W.F. Sangrey, and W. M. White, Sources of error in external calibration ICP-MS analysis of geological samples and an improved non-linear drift correction, *Spectrochim. Acta Electron., 48B*, E487-E506, 1993.

Christie, D. M., R. A. Duncan, A. R. McBirney, M. A. Richards, W. M. White, K. S. Harpp, and C. G. Fox, Drowned islands downstream from the Galápagos hotspot imply extended speciation times, *Nature, 355*, 246-248, 1992.

Colinvaux, P. A., The Galapagos climate: present and past, in *Key Environments: Galapagos*, edited by C. Perry, p. 15-41, Pergamon, New York, 1984.

Cox, A. and G.B. Dalrymple, Paleomagnetism and potassium-argon ages of some volcanic rocks from the Galápagos Islands, *Nature, 209*, 776-777, 1966.

Cullen, A. B., Geology and Petrology of Isla Pinta, Galápagos, M.S. thesis, 77 pp., Univ. of Oreg., Eugene, 1985.

Cullen, A., and A. R. McBirney, The volcanic geology and petrology of Isla Pinta, Galápagos Archipelago, *Geol. Soc. Am. Bull., 98*, 294-301, 1987.

Cullen, A. B., A. R. McBirney, and R. D. Rogers, Structural controls on the morphology of Galápagos shields, *J. Volcanol. Geotherm. Res., 34*, 143-151, 1987.

Cullen, A., E. Vicenzi, and A. R. McBirney, Plagioclase-ultraphyric basalts of the Galápagos Archipelago, *J. Volcanol. Geotherm. Res., 37*, 325-337, 1989.

Dalymple, G. B., and M. A. Lanphere, *Potassium-Argon Dating*, W. H. Freeman, New York, 1969.

Darwin, C., *The Voyage of the Beagle*, 524 pp., Doubleday, New York, 1860.

Delaney, J. R., W. E. Colony, T. M. Gerlach, and B. E. Nordlie, Geology of the Volcan Chico area on Sierra Negra Volcano, Galápagos Islands, *Geol. Soc. Am. Bull., 84*, 2455-2470, 1973.

Duncan, R. A., M. T. McCulloch, H. G. Barczus, and D. R. Nelson, Plume versus lithopheric sources for the melts at Ua Pou, Marquesas Island, *Nature, 303*, 142-146, 1986.

Emerman, S. H. and D. L. Turcotte, Stagnation flow with a temperature-dependent viscosity, *J. Fluid Mech., 127*, 507-517, 1983.

Gallahan, W. E., and R. L. Nielsen, The partitioning of Sc, Y and the rare earth elements between high-Ca pyroxene and natural mafic to intermediate lavas at 1 atmosphere, *Geochim. Cosmochim. Acta, 56*, 2387-2404, 1992.

Geist, D. J., An appraisal of melting processes and the Galápagos hotspot: Major and trace element evidence, *J. Volcanol. Geotherm. Res., 52*, 65-82, 1992.

Geist, D. J., A. R. McBirney, and R. A. Duncan, Geology and petrogenesis of lavas from San Cristobal, Galápagos Archipelago, *Geol. Soc. Am. Bull., 97*, 555-566, 1985*a*.

Geist, D. J., A. R. McBirney, and R. A. Duncan, Geology of Sante Fe Island: the oldest Galápagos volcano, *J. Volcanol. Geotherm. Res., 26*, 203-212, 1985*b*.

Geist, D. J., W. M. White, and A. R. McBirney, Plume-asthenosphere mixing beneath the Galápagos Archipelago., *Nature, 333*, 657-660, 1988.

Gillot, P.-Y. and P. Nativel, Eruptive history of the Piton de la Fournaise volcano, Reunion Island, Indian Ocean, *J. Volcanol. Geotherm. Res., 36*, 53-66, 1989.

Griffiths, R. W., The differing effects of compositional and thermal buoyancies on the evolution of mantle diapirs, *Phys. Earth Planet. Inter., 43*, 261-273, 1986.

Gripp, A. E., and R. G. Gordon, Current plate velocities relative to hotspots incorporating the NUVEL-1 global plate model, *Geophys. Res. Lett., 17*, 1109-1112, 1990.

Hall, M. L., Origin of Española Island and the age of terrestrial life on the Galápagos Islands, *Science, 221*, 545-547, 1983.

Hanson, G. N., Geochemical evolution of the suboceanic mantle, *J. Geol. Soc. London, 134*, 1-19, 1977.

Hanson, G. N., and C. H. Langmuir, Modelling of major elements in mantle-melt systems using trace element approaches., *Geochim. Cosmochim. Acta, 42*, 725-741, 1978.

Harpp, K. S., W. M. White, and R. A. Duncan, Geochemistry of the Wolf-Darwin Lineament and ridge-plume interaction in the Galápagos, *Geol. Soc. Aust. Abtr., 27*, 44, 1990.

Hart, S. R., and C. Brooks, Clinopyroxene-matrix partitioning of K, Rb, Cs, Sr, and Ba, *Geochim. Cosmochim. Acta, 38*, 1799-1806, 1974.

Hey, R., Tectonic evolution of the Cocos-Nazca spreading center, *Geol. Soc. Am. Bull., 88*, 1404-1420, 1977.

Jaques, A. L., and D. H. Green, Anhydrous melting of peridotite at 0-15 Kb pressure and the genesis of tholeiitic basalts, *Contrib. Mineral. Petrol., 73*, 287-310, 1980.

Klein, E. M., and C. H. Langmuir, Ocean ridge basalt chemistry, axial depth, crustal thickness and temperature variations in the mantle, *J. Geophys. Res., 92*, 8089-8115, 1987.

Klein, E. M., and C. H. Langmuir, Local versus global variations in ocean ridge basalt composition: A reply, *J. Geophys. Res., 94*, 4241-4252, 1989.

Levi, S., H. Audunsson, R.A. Duncan, L. Kristjansson, P.-Y. Gillot, and S.K. Jakobsson, Late Pleistocene geomagnetic excursion in Iceland lavas: Confirmation of the Laschamp excursion, *Earth Planet. Sci. Lett., 96*, 443-457, 1990.

Lindstrom, M. M., Geochemical studies of volcanic rocks from Pinzón and Santiago islands, Galápagos Archipelago, Ph.D. disseration, 174 pp., Univ. of Oreg, Eugene, 1976.

Macdonald, G. A., and T. Katsura, Chemical composition of Hawaiian lavas, *J. Petrol., 5*, 82-133, 1964.

Malfait, B. T., and M. G. Dinkerman, Circum-Pacific tectonic and igneous activity and the evolution of the Caribbean plate, *Geol. Soc. Am. Bull., 83*, 251-272, 1972.

McBirney, A. R., Differentiated rocks of the Galápagos hotspot, *J. Geol. Soc. London*, in press, 1993.

McBirney, A. R., A. B. Cullen, D. Geist, E. P. Vicenzi, R. A. Duncan, M. L. Hall, and M. Estrella, The Galápagos Volcano Alcedo: A unique ocean caldera, *J. Volcanol. Geotherm. Res., 26*, 173-177, 1985.

McBirney, A. R., and H. Williams, *Geology and Petrology of the Galápagos Islands, Geol. Soc. Am. Mem. 118*, pp. 197, Geol. Soc. Am., Boulder, 1969.

Minster, J. B., and T. H. Jordan, Present-day plate motions, *J. Geophys. Res., 83*, 5331-5354, 1978.

Moore, J. G., Subsidence of the Hawaiian Ridge, *U.S. Geol. Surv. Prof. Pap., 1350*, 85-100, 1987.

Morgan, W. J., Convection plumes in the lower mantle., *Nature, 230*, 42-43, 1971.

Morgan, W. J., Rodriguez, Darwin, Amsterdam..., A second type of hotspot island, *J. Geophys. Res., 83*, 5355-5360, 1978.

Morris, J. D., and S. R. Hart, Isotopic and incompatible element constraints on the genesis of arc volcanics from Cold Bay and Amak Island, Aleutians, and implications for mantle structure, *Geochim. Cosmochim. Acta, 47*, 2015-2030, 1983.

Nakamura, N., Determination of REE, Ba, Fe, Mg, Na and K in carbonaceous and ordinary chondrites, *Geochim. Cosmochim. Acta, 38*, 757-775, 1974.

Prestvik, T., and R.A. Duncan, The geology and age of Peter I Oy, Antarctica, *Polar Res., 9*, 89-98, 1991.

Richards, M. A., and R. W. Griffiths, Thermal entrainment by deflected mantle plumes, *Nature, 342*, 900-902, 1989.

Rowland, S. K., and D. C. Munro, The caldera of Volcan Fernandina: A remote sensing study of its structure and recent activity, *Bull. Volcanol., 55*, 97-109, 1992.

Salters, V. J. M., and S. R. Hart, The Hf-paradox, and the role of garnet in the MORB source, *Nature, 342*, 420-422, 1989.

Schilling, J.-G., Icelandic mantle plume: Geochemical evidence along the Reykjanes Ridge., *Nature, 242*, 565-571, 1973.

Schilling, J.-G., Fluxes and excess temperatures of mantle plumes inferred from their interaction with migrating mid-ocean ridges, *Nature, 352*, 397-403, 1991.

Schilling, J.-G., R. N. Anderson, and P. Vogt, Rare earth, Fe and Ti variations along the Galápagos spreading centre, and their relationship to the Galápagos mantle plume, *Nature, 261*, 108-113, 1976.

Schilling, J.-G., R. H. Kingsley, and J. D. Devine, Galápagos hot spot–spreading center system, 1, Spatial petrological and geochemical variations (83°W-101°W), *J. Geophys. Res., 87*, 5593-5610, 1982.

Shimizu, H., A. Masuda, and N. Masui, Rare-earth element geochemistry of volcanic rocks from the Galápagos Islands, *Geochemical J., 15*, 81-93, 1981.

Shimizu, N., An isotope dilution technique for analysis of the rare earth elements, *Year Book Carnegie Inst. Washington, 73*, 941-943, 1974.

Simkin, T., Geology of the Galapagos Islands, in *Key Environments: Galapagos*, edited by R. Perry, pp. 15-41, Pergamon, New York, 1984.

Simkin, T., and K. A. Howard, Caldera collapse in the Galápagos Islands,

1968, *Science, 169*, 429-437, 1970.
Simkin, T., L. Siebert, L. McClelland, D. Bridge, C. Newhall, and J. H. Latter, *Volcanos of the World*, 232 pp., Smithsonian Institution, Washington, D. C., 1981.
Sinton, J. M., and R. Detrick, Mid-ocean ridge magma chambers, *J. Geophys. Res.*, *97*, 197-216, 1992.
Stille, P., D. M. Unruh, and M. Tatsumoto, Pb, Sr, Nd, and Hf isotopic constraints on the origin of Hawaiian basalts and evidence for a unique mantle source, *Geochim. Cosmochim. Acta*, *50*, 2303-2320, 1986.
Swanson, F. J., H. W. Baitis, J. Lexa, and J. Dymond, Geology of Santiago, Rábida, and Pinzón Islands, Galápagos, *Geol. Soc. Am. Bull.*, *85*, 1803-1810, 1974.
van Andel, T. H., G. R. Heath, B. T. Malfait, D. F. Heinrichs, and J. I. Ewing, Tectonics of the Panama Basin, eastern equatorial Pacific, *Geol. Soc. Am. Bull.*, *82*, 1482-1504, 1971.
van Andel, T., et al., *Initial Reports of the Deep Sea Drilling Project*, 949 pp., U. S. Goverment Printing Office, Washington, D.C., 1973.
Verma, S. P., and J.-G. Schilling, Galápagos hot spot–spreading center system, 2, $^{87}Sr/^{86}Sr$ and large ion lithophile element variations (85°W-101°W), *J. Geophys. Res.*, *87*, 10838-10856, 1982.
Verma, S. P., J.-G. Schilling, and D. G. Waggoner, Neodymium isotopic evidence for Galápagos hotspot-spreading centre system evolution, *Nature*, *306*, 654-657, 1983.
Vicenzi, E., The geology, petrology, and petrogenesis of Isla Marchena, Galápagos Archipelago, M.S. thesis, 96 pp., Univ. of Oreg, Eugene, 1985.
Vicenzi, E. P., A. R. McBirney, W. M. White, and M. Hamilton, The geology and geochemistry of Isla Marchena, Galápagos Archipelago: An ocean island adjacent to a mid-ocean ridge, *J. Volcanol. Geotherm. Res.*, *40*, 291-315, 1990.
Vogt, P. R., Volcano height and plate thickness, *Earth Planet. Sci. Lett.*, *23*, 337-348, 1974.
Walker, R. J., R. W. Carlson, S. B. Shirey, and F. R. Boyd, Os, Sr, Nd, and Pb isotope systematics of southern African peridotite xenoliths: Implications for the chemical evolution of the subcontinental mantle, *Geochim. Cosmochim. Acta*, *53*, 1583-1595, 1989.
White, W. M., and B. Dupré, Sediment subduction and magma genesis in the Lesser Antilles: Isotopic and trace element constraints, *J. Geophys. Res.*, *91*, 5927-5941, 1986.
White, W. M., and A. W. Hofmann, Geochemistry of the Galápagos Islands: Implications for mantle dynamics and evolution., *Year Book Carnegie Inst. Washington*, *77*, 596-606, 1978.
White, W. M., and A. W. Hofmann, Sr and Nd isotope geochemistry of oceanic basalts and mantle geochemistry, *Nature*, *296*, 821-825, 1982.
White, W. M., and P. J. Patchett, Hf-Nd-Sr and incompatible-element abundances in island arcs: Implications for magma origins and crust-mantle evolution, *Earth Planet. Sci. Lett.*, *67*, 167-185, 1984.
Whitford, D. J., W. M. White, A. W. Hofmann, and D. E. James, Separation and isotopic analysis of neodymium, *Year Book Carnegie Inst. Washington*, *77*, 620-623, 1978.
Wright, T. L., and R. S. Fiske, Origin of the differentiated and hybrid lavas of Kilauea Volcano, Hawaii, *J. Petrol.*, *12*, 1-65, 1971.
Wyllie, P. J., Solidus curves, mantle plumes, and magma generation beneath Hawaii, *J. Geophys. Res.*, *93*, 4171-4181, 1988.
Yoder, H. S., and C. E. Tilley, Origin of basalt magmas: an experimental study of natural and synthetic rock systems., *J. Petrol.*, *3*, 342-532, 1962.
Zindler, A., S. R. Hart, F. A. Frey, and S. P. Jakobsson, Nd and Sm isotope ratios and rare earth element abundances in Reykjanes Peninsula basalts; Evidence for mantle heterogeniety beneath Iceland, *Earth Planet. Sci. Lett.*, *45*, 249-262, 1979.
Zindler, A., H. Staudigel, and R. Batiza, Isotope and trace element geochemistry of young Pacific seamounts: Implications for the scale of upper mantle heterogeneity, *Earth Planet. Sci. Lett.*, *70*, 175-195, 1984.

R. A. Duncan, College of Oceanography, Oregon State University, Corvallis, OR 97331.

A. R. McBirney, Center for Volcanology, University of Oregon, Eugene, OR 97403.

W. M. White, Dept. of Geological Sciences, Cornell University, Ithaca, NY 14853.

(Received August 3, 1992;
revised July 15, 1993;
accepted July 21, 1993.)